Assessing Practical Identifiability during Calibration and Cross-Validation of a Structured Model for High-Solids Anaerobic Digestion

Vicente Pastor-Poquet [a,b,*], Stefano Papirio [c], Jérôme Harmand [b], Jean-Philippe Steyer [b], Eric Trably [b], Renaud Escudié [b], and Giovanni Esposito [c]

[a] Department of Civil and Mechanical Engineering, University of Cassino and Southern Lazio, via Di Biasio 43, 03043 Cassino (FR), Italy

* Corresponding author. E-mail: vicente.pastor.poquet@gmail.com

[b] LBE, Univ. Montpellier, INRA, 102 Avenue des Etangs, 11100, Narbonne, France

[c] Department of Civil, Architectural and Environmental Engineering, University of Napoli Federico II, via Claudio 21, 80125 Napoli, Italy

ABSTRACT

High-solids anaerobic digestion (HS-AD) of the organic fraction of municipal solid waste (OFMSW) is operated at a total solid (TS) content ≥ 10 % to enhance the waste treatment economy, though it might be associated to free ammonia (NH_3) inhibition. This study aimed to calibrate and cross-validate a HS-AD model for homogenized reactors in order to assess the effects of high NH_3 levels in HS-AD of OFMSW, but also to evaluate the suitability of the reversible non-competitive inhibition function to reproduce the effect of NH_3 on the main acetogenic and methanogenic populations. The practical identifiability of structural/biochemical parameters (i.e. 35) and initial conditions (i.e. 32) was evaluated using batch experiments at different TS and/or

inoculum-to-substrate ratios. Variance-based global sensitivity analysis and approximate Bayesian computation were used for parameter optimization. The experimental data in this study permitted to estimate up to 8 biochemical parameters, whereas the rest of parameters and biomass contents were poorly identifiable. The study also showed the relatively high levels of NH_3 (i.e. up to 2.3 g N/L) and ionic strength (i.e. up to 0.9 M) when increasing TS in HS-AD of OFMSW. However, the NH_3 non-competitive function was unable to capture the acetogenic/methanogenic inhibition. Therefore, the calibration emphasized the need for target-oriented experimental data to enhance the practical identifiability and the predictive capabilities of structured HS-AD models, but also the need for further testing the NH_3 inhibition function used in these simulations.

Keywords: High-solids Anaerobic Digestion Model; Ammonia Inhibition; Ionic Strength; Global Sensitivity Analysis; Approximate Bayesian Computation.

1 INTRODUCTION

High-solids anaerobic digestion (HS-AD) of the organic fraction of municipal solid waste (OFMSW) is operated at total solids (TS) ≥ 10 % to minimize the reactor volume, the water addition and the digestate dewatering (Pastor-Poquet et al., 2019a). HS-AD can also lead up to 80 % TS removal, easing the digestate post-treatment. However, HS-AD of OFMSW is usually associated to free ammonia (NH_3) inhibition, resulting in volatile fatty acids (VFA) accumulation. NH_3 affects both acetoclastic and hydrogenotrophic methanogens but also the rest of VFA degraders (acetogens) in anaerobic digestion (AD), being the inhibition related to the operative parameters (i.e. temperature and pH) and the biomass acclimation (Rajagopal et al., 2013).

Adding lignocellulosic materials to OFMSW permits to minimize the buildup of total ammonia nitrogen (TAN), while their low hydrolysis rates permit to increase the TS content and to counteract the VFA accumulation in HS-AD (Capson-Tojo et al., 2017; Pastor-Poquet et al., 2019a). However, including lignocellulosic waste in OFMSW depends on the season or the local waste management strategy. Whether or not a lignocellulosic co-substrate is used, understanding the effects of NH_3 inhibition is crucial to optimize HS-AD of OFMSW.

A HS-AD model was recently developed for homogenized reactors to evaluate the NH_3 inhibition in HS-AD of OFMSW (Pastor-Poquet et al., 2018, 2019b). This structured model, based on the Anaerobic Digestion Model No. 1 (ADM1) (Batstone et al., 2002), gathers the main bio-physical-chemical mechanisms in HS-AD. In the HS-AD model, apparent (i.e. kmol/kg H_2O) instead of global (i.e. kmol/kg) concentrations determine

64 the effect of TS upon solutes, as a consequence of the low water content within HS-AD.
65 Meanwhile, an extended set of mass balances allows the simulation of the organic mass
66 removal from the biogas production. A liquid solution 'non-ideality' subroutine was
67 subsequently included in the model as a function of the ionic strength (*I*), since 'non-
68 ideality' determines the pH, CO_2 liquid-gas transfer and NH_3 inhibition in HS-AD
69 (Pastor-Poquet et al., 2019b). As a preliminary assumption, the HS-AD model included
70 a reversible non-competitive inhibition function by NH_3 (I_{nh3}) [Equation 1] in the
71 biochemical rates of acetogenic and methanogenic populations, a mathematical resource
72 commonly used in structured AD models (Astals et al., 2018).
73

$$I_{nh3} = \frac{K_{i,Snh3}}{K_{i,Snh3} + S_{nh3,App}} \quad (1)$$

74

75 Simulating the NH_3 inhibition at high TS with the HS-AD model requires an adequate
76 set of input parameters, θ, to be estimated by calibration (Pastor-Poquet et al., 2018,
77 2019b). θ includes both the structural/biochemical parameters, θ_P, and the initial and
78 influent conditions, θ_B: $\theta = (\theta_P, \theta_B)$. Nonetheless, calibration of structured AD models is
79 not trivial due to the equation complexity and large number of θ involved (Dochain &
80 Vanrolleghem, 2001; Donoso-Bravo et al., 2011).
81

82 To calibrate a mathematical model, θ must be structurally and practically identifiable,
83 instead of correlated. The θ structural identifiability is theoretically assessed, assuming
84 noise-free experimental data and error-free model structure. Noteworthy, nearly all θ in
85 ADM1 are (locally) structurally identifiable (Nimmegeers et al., 2017). This is a
86 prerequisite to assess the θ practical identifiability and calibrate the HS-AD model using

87 'imperfect' experimental data. Unfortunately, the reduced number of experimental data
88 often available and/or the presence of experimental errors yield non-identifiable
89 parameters; i.e. parameters that cannot be uniquely estimated. These are known as
90 practical identifiability issues.
91
92 Calibration usually consists of minimizing an objective function, $J(\theta)$, that condenses
93 the 'goodness of fitting' between the experimental data, y, and the model outputs, $y^{sim}(\theta)$,
94 being these a function of N input parameters, θ (Dochain & Vanrolleghem, 2001;
95 Flotats et al., 2010). Several $J(\theta)$ can be used to calibrate AD models as the weighted
96 sum of squares or any user-defined alternative (Donoso-Bravo et al., 2011; Ratto et al.,
97 2001). Assuming the existence of a global minimum (optimum) for an objective
98 function, $J(\theta_{opt})$, this value is reached using the optimal set of input parameters, θ_{opt}.
99
100 Practical identifiability issues commonly translate into $J(\theta)$ showing many local
101 optimums and/or flat valleys, where the precise value of θ cannot be easily determined
102 (Guisasola et al., 2006; Rodriguez-Fernandez et al., 2006). Thus, only practical
103 identification of a reduced θ subset (i.e. $N' < N$) is often possible for ADM1-based
104 models (Nimmegeers et al., 2017). This is called model over-parameterization, where
105 the modification of two individual θ, θ_i (with $i = 1, \ldots, N$), can lead to a similar model
106 output. Particularly, when using batch experiments – highly dependent on the initial
107 conditions – to calibrate AD models, different sets of experimental conditions, including
108 different inoculum-to-substrate ratios (ISR), are required to reduce the θ correlation
109 (Donoso-Bravo et al., 2011; Flotats et al., 2010).
110

Two main approaches can be used to calibrate complex models: the Bayesian and the frequentist. The frequentist approach searches for optimal θ values, θ_{opt}, whereas the Bayesian approach considers θ_{opt} as probabilistic distributions conditioned on the experimental data, $p(\theta_{opt}|y)$, instead of single values (Ratto et al., 2001; Rodriguez-Fernandez et al., 2006; Saltelli et al., 2006). In both approaches, when facing over-parameterization, it must be assessed which θ_i significantly influence $y^{sim}(\theta)$ (sensitivity analysis) and need to be adequately calibrated.

ADM1-based models contain several θ_P (i.e. ≥ 35) and θ_B (i.e. ≥ 24). θ_P might be obtained from literature, though a different model structure – from where these θ_P were obtained – potentially influences the optimal θ_P values/distributions (Pastor-Poquet et al., 2019b). On the other hand, θ_B might not be easily determined due to the lack of experimental data or the difficulties to translate the data into adequate model units (Donoso-Bravo et al., 2011; Flotats et al., 2003).

Parameter inference based on the Bayes' theorem [Equation 2] is particularly suited to calibrate structured AD models since it can deal with complex $J(\theta)$ showing several optima or flat geometries, where frequentist inference might not be well suited (Kennedy & O'Hagan, 2001; Toni & Stumpf, 2010). In Bayesian inference, the prior parameter distribution, $p(\theta)$, is sampled to obtain the posterior parameter distribution, $p(\theta|y)$, conditioned on the experimental data, y, and the likelihood function, $p(y|\theta)$, while $p(y)$ can be considered as a normalizing constant. Importantly, any user-defined $J(\theta)$ arising from $p(y|\theta)$ can be used in 'informal' statistical approaches [Equation 3], as

variance-based global sensitivity analysis (GSA) and approximate Bayesian computation (ABC) (Donoso-Bravo et al., 2011; Nott et al., 2012).

$$p(\theta|y) = \frac{p(y|\theta)p(\theta)}{p(y)} \quad (2)$$

$$J(\theta) = f(p(y|\theta)) \quad (3)$$

Variance-based GSA provides an appropriate assessment about the potentiality of θ_i to influence the model outputs and the correlations existing with the rest of θ, θ_j (with j = 1, …, N and $i \neq j$) (Kennedy & Petropoulos, 2017; Oakley & O'Hagan, 2004). Similarly, ABC permits also to highlight practical identifiability issues yielding simultaneously the most likely $p(\theta|y)$ (Beaumont et al., 2009; Filippi et al., 2013; Toni & Stumpf, 2010). As main disadvantage, Bayesian inference is often computationally intensive.

The mathematical performance of the HS-AD model was previously verified, though the model was only validated for a single HS-AD batch experiment due to the elevated number of θ requiring calibration (i.e. > 30) (Pastor-Poquet et al., 2018, 2019b). Instead, this study aimed to fully calibrate and cross-validate the HS-AD model to simulate the effect of high NH_3 levels in HS-AD of OFMSW, while testing the non-competitive NH_3 inhibition function [Equation 1] on the main acetogenic/methanogenic populations. In particular, this study assessed the practical identifiability of 35 θ_P and 32 θ_B, by using nine HS-AD batch digesters at different TS and/or ISR as a source of experimental data. Identifiability was assessed by variance-based GSA and ABC permitting to approximate also $p(\theta|y)$. Importantly, the proposed methodology can be easily readapted to account for further HS-AD datasets (e.g. batch, continuous) and/or model configurations.

156

157 **2 METHODOLOGY**

158 **2.1 Experimental Data**

159 To calibrate and cross-validate the HS-AD model, while further evaluating the effects of
160 increasing the initial TS content on HS-AD simulations, four different batch
161 experiments were used at thermophilic (55ºC) conditions from 10 to 30 % TS [Table 1].
162 The laboratory-scale reactor design volume ($V_{Reactor}$) was either 160 or 280 mL for the
163 different experiments. In all experiments, centrifuged inoculum was used to increase
164 simultaneously the initial TS and ISR. These small-scale digesters were manually
165 shaken when the biogas production was measured. The batch experiments are described
166 next, whereas a thorough description of these experiments and the bio-physical-
167 chemical analyses performed was reported elsewhere (Pastor-Poquet et al., 2019a).

168

169 Experiment 1 consisted of a sacrifice test for mono-digestion of OFMSW using ISR =
170 1.00 g VS/g VS. In this experiment, the main physical-chemical dynamics (i.e. biogas
171 production and composition, TS, VS, VFA, TAN, and mono-valent ions) were
172 evaluated at different operational times. In Experiments 2 to 4, the biogas production
173 and composition were measured at different experimental times, whereas the rest of
174 physical-chemical analyses (i.e. TS, VS, VFA, TAN and ions) were only performed
175 before starting and after ending each experiment. Non-sacrifice experiments included
176 mono-digestion of OFMSW using ISR = 1.50 g VS/g VS (Experiment 2) and ISR =
177 0.50 g VS/g VS (Experiment 3), but also co-digestion of OFMSW and beech sawdust
178 using ISR = 0.16 g VS/g VS (Experiment 4).

179

Within Experiments 2 and 4, different initial TS contents – dilutions – were evaluated, though all the initial batch conditions contained exactly the same amount of substrate and centrifuged inoculum. Briefly: 1) the inoculum was centrifuged; 2) the same amount of substrate and inoculum was added to each bottle; 3) distilled water was added to reach the different TS contents; and 4) each bottle was manually homogenized. This strategy was aimed to use the mass balances among the different initial TS conditions, as explained in Section 2.3.1, since soluble materials were partially removed when centrifuging the inoculum. In total, nine different HS-AD batch conditions were assessed at different TS, ISR and/or co-digestion ratios, subsequently named as "Batch No. 1 to 9" [Table 1].

2.2 HS-AD Model

The HS-AD model included the main biochemical rates of Pastor-Poquet et al. (2018), though some minor modifications were also implemented [Table 2]. Firstly, a reversible non-competitive NH_3 inhibition function [Equation 1] was included in the valeric (S_{va}), butyric (S_{bu}), propionic (S_{pro}), and hydrogen (S_{h2}) uptake rates, similarly to the NH_3 (S_{nh3}) inhibition on the acetate (S_{ac}) uptake, aiming to simulate the VFA accumulation observed in HS-AD experiments likely consequence of the NH_3 buildup (Pastor-Poquet et al., 2019a). Secondly, carbohydrates (X_{ch}) were split into readily-biodegradable ($X_{ch,fast}$) and slowly-biodegradable ($X_{ch,slow}$) to simulate the relatively lower hydrolysis rates of sawdust and the longer methane production observed in co-digestion experiments (i.e. ≥ 200 d) [Table 1]. Importantly, the hydrolysis of both $X_{ch,fast}$ and $X_{ch,slow}$ pooled into soluble sugars (S_{su}).

204 **2.3 Model Calibration and Validation**

205 A common set of biochemical parameters was used for all HS-AD simulations at
206 different ISR and/or TS. All biochemical parameters for thermophilic (55ºC) AD were
207 extracted from Batstone et al. (2002), though some of those needed to be calibrated (i.e.
208 θ_P) to improve the model fitting. The initial conditions of the batch experiments were
209 predefined according to the experimental data available, as described by Pastor-Poquet
210 et al. (2018) and also mentioned next. Moreover, different ranges of initial biomass
211 concentrations were used (i.e. θ_B) to assess the potential interrelationship of θ_B with θ_P
212 in batch experiments.
213

214 **2.3.1 Initial Conditions**

215 The initial conditions used for each batch simulation are shown in Table 3. Since the
216 same amount of substrate and inoculum was used along different initial TS contents in
217 Experiment 2, but also in Experiment 4, mass balances were used to reduce the number
218 of 'unknown' initial conditions [Table 1]. To use mass balances, the anaerobic
219 biodegradability (BD) of each substrate-inoculum mixture in Experiment 2 and
220 Experiment 4 was assumed constant, whereas the soluble (S) and particulate (X)
221 components were assumed proportional, among the different TS contents. With these
222 assumptions, mass balances permitted to extrapolate the molar and chemical oxygen
223 demand (COD) concentrations as a function of the initial reactor content mass (M_{Global}),
224 reactor content specific weight (ρ_{Global}) and reactor content volume (V_{Global}). For
225 example, the concentration of acetoclastic methanogens (X_{ac}) in Batch No. 3 was
226 approximated from Batch No. 2 as: $X_{ac,Batch3} = X_{ac,Batch2} \cdot V_{Global,Batch2}/V_{Global,Batch3}$.
227

The nitrogen content of soluble (S_i) and particulate (X_i) inert in each substrate-inoculum mixture ($N_{i,subs}$) determined the initial protein (X_{pr}) + amino-acid (S_{aa}) content, according to the nitrogen balance, as shown elsewhere (Pastor-Poquet et al., 2018). Thus, $N_{i,subs}$ was different for each batch experiment [Table 3]. On the other hand, despite the initial conditions of batch experiments were maintained for all the simulations, different biomass concentrations (i.e. degraders of sugars, X_{su}; amino acids, X_{aa}; long-chain fatty acids, X_{fa}; valerate, X_{c5}; butyrate, X_{bu}; propionate, X_{pro}; acetate, X_{ac}; and hydrogen, X_{h2}) were also assessed, as mentioned before. Since mass balances were used among different TS in Experiments 2 and 4, only the initial conditions of Batch No. 1, 2, 6 and 7 [Table 1] were evaluated.

2.3.2 Biochemical Parameters, Biomass Concentrations and Calibration Ranges

The modified biochemical parameters (θ_P) and modified biomass concentrations (θ_B) in this study, including their initial values and potential variability ranges, are shown in Table 4. In total, 35 θ_P and 32 θ_B were evaluated. θ_P related to the hydrolysis, sugar fractioning (f_{su}), maximum growth rate (k_m) and half-saturation constant (K_S), but also the pH, NH_3 and H_2 inhibition constants (K_i), since all these θ_P are simultaneously associated to the substrate under study, are correlated among themselves, and strongly regulate the biogas production/composition from solid substrates (Batstone et al., 2002; Garcia-Gen et al., 2015). On the other hand, θ_B included all the initial biomass concentrations in the HS-AD simulations (i.e. X_{su}, X_{aa}, X_{fa}, X_{c5}, X_{bu}, X_{pro}, X_{ac} and X_{h2}), as these concentrations might not only strongly influence the biogas production during the initial days of batch experiments, but might also be potentially interrelated among themselves and/or to the previous θ_P.

252

253 The sugars uptake yields butyrate ($f_{bu,su}$), propionate ($f_{pro,su}$), acetate ($f_{ac,su}$) and hydrogen
254 ($f_{h2,su}$) as COD fractions in ADM1. Therefore, a maximum of three fractions can be
255 selected simultaneously to fulfill the COD balance: $f_{bu,su} + f_{pro,su} + f_{ac,su} + f_{h2,su} = 1$. In
256 this study, $f_{bu,su}$, $f_{ac,su}$ and $f_{h2,su}$ were selected, while $f_{pro,su}$ was recalculated: $f_{pro,su} = 1 -$
257 $f_{bu,su} - f_{ac,su} - f_{h2,su}$. Importantly, further structural parameters and initial conditions need
258 to be induced in the HS-AD model as, for example, the amino-acid (AA, S_{aa})
259 fractioning and the biomass yield coefficients (Y_b), though these were not assessed here
260 aiming to reduce the problem under study. In either case, the proposed methodology for
261 calibration/validation can easily include any further θ.

262

263 Variability ranges for structural parameters are suggested in ADM1 (Batstone et al.,
264 2002). However, considerably wider ranges were assessed in this study to emphasize
265 the absence of prior knowledge about the optimal values. For simplicity, all θ_P were
266 allowed to vary by 90 % from their initial values, $\theta_{P,0}$: $(1 - 0.9) \cdot \theta_{P,0} \leq \theta_P \leq (1 +$
267 $0.9) \cdot \theta_{P,0}$; uniform $p(\theta_P)$ [Table 4]. As the only exception, the lower pH threshold for
268 acetoclastic methanogens ($pH_{LL,ac}$) was bounded between a pH value where
269 methanogenesis potentially collapses (i.e. ≤ 5.0) and the upper pH threshold for
270 acetoclastic methanogens ($pH_{UL,ac}$, i.e. 7.0), to maintain the suitability of the Hill
271 function to simulate the pH inhibition [Table 2].

272

273 Different methods are available to approximate the initial conditions (i.e. biomass
274 concentrations) in batch simulations as, for example, simulating a continuous reactor
275 fed with exactly the same substrate until reaching steady state, and then use these steady

conditions to initialize the batch simulations (Dochain & Vanrolleghem, 2001; Donoso-Bravo et al., 2011). However, since the inoculum was centrifuged right before setting the batch experiments in this study, absence of prior knowledge about the initial biomass concentrations was preferred. To explore homogeneously different orders of magnitude in the biomass concentrations (often $0 < \theta_B < 1$ kmol COD/m^3), the logarithm-transformed θ_B were allowed to vary by 50 % from their initial values, $\theta_{B,0}$: $(1 + 0.5) \cdot log_{10}(\theta_{B,0}) \leq log_{10}(\theta_B) \leq (1 - 0.5) \cdot log_{10}(\theta_{B,0})$; uniform $p(log_{10}(\theta_B))$ [Table 4].

2.3.3 Objective Function

The weighted sum of squares between all the available experimental and the corresponding simulated values was used as objective function, $J(\theta)$ [Equation 4]. $J(\theta)$ was adapted from Flotats et al. (2003) to assess the model 'goodness of fitting', being: θ the structural parameters and/or initial conditions implemented in the HS-AD model; R the number of batch simulations; D the number of experimental datasets; t_{exp} the experimental time of each batch experiment; $y_{i,j,t}$ the experimental measurements; $y_{i,j,t}^{sim}(\theta)$ the simulated values; and $w_{i,j}$ the weighting coefficients – calculated as a function of the average experimental data, $\bar{y}_{i,j}$ [Equation 5]. With this approach, $J(\theta)$ was lower-bounded by the – preliminarily unknown – global minimum: $J(\theta) \geq J(\theta_{opt})$.

$$J(\theta) = \sum_{i=1}^{R} \sum_{j=1}^{D} \sum_{t=t_1}^{t_{exp}} w_{i,j} \left(y_{i,j,t} - y_{i,j,t}^{sim}(\theta) \right)^2 \quad (4)$$

$$w_{i,j} = \frac{1}{\sum_{t=t_1}^{t_{exp}} \left(y_{i,j,t} - \bar{y}_{i,j} \right)^2} \quad (5)$$

Noteworthy, only 6 out of 9 experimental conditions were used to calculate $J(\theta)$ in this study: Batch No. 1, 3, 5, 6, 7 and 9 [Table 1]. Meanwhile, 3 out of 9 experimental

297 conditions were used for cross-validation: Batch No. 2, 4 and 8 [Table 1]. Other
298 experimental combinations could be used for calibration/cross-validation as, for
299 example, Batch No. 2, 4, 5, 7 and 8 for calibration and Batch No. 1, 3, 6 and 9 for cross-
300 validation. However, the configuration used in this study permitted to include the most
301 extreme HS-AD conditions for model calibration (i.e. TS ≤ 10 %, TS ≥ 30 %), while
302 intermediate conditions (i.e. 10 ≤ TS ≤ 30 %) were used for cross-validation. This
303 strategy also aimed to enhance the number of experimental data used for calibration and
304 to ensure the most diverse operative conditions where θ might be representative.
305 Additionally, the proposed configuration included the most informative dataset (i.e.
306 Batch No. 1) to increase the complexity of $J(\theta)$ and remove identifiability issues related
307 to the lack of bio-physical-chemical dynamics in the overall dataset, as further discussed
308 in Section 3.1.3.
309

310 **2.3.4 Global Sensitivity Analysis**

311 GSA was aimed to highlight the most influential θ to be calibrated with the available set
312 of experimental data. For GSA, multiple θ combinations were used to evaluate $J(\theta)$
313 [Equation 4]. Latin-hypercube sampling (LHS) served to explore the global θ space
314 (Solon et al., 2015). Subsequently, $J(\theta)$ arrays and their corresponding θ were assessed
315 by the GSA engine of Kennedy and O'Hagan (2001) and Oakley and O'Hagan (2004).
316 The GSA engine calculates the individual (IE) and global (GE) effects of θ_i upon the
317 global model output (e.g. $p(y|\theta)$, $J(\theta)$) variance. On the other hand, the GSA engine
318 provides also all the double correlations between θ_i and θ_j (i.e. $\theta_i \cdot \theta_j$, being $i \neq j$). Both
319 IE and $\theta_i \cdot \theta_j$ are expressed as a percentage of the global variance explained. Thus, θ_i
320 showing a relatively low IE are associated to poor practical identifiability, since these θ_i

influence minimally the model output. Meanwhile, GE comprises IE, the double correlations $\theta_i \cdot \theta_j$ and all the rest of multiple correlations for a single θ_i. Therefore, GE itself should not be used to assess the identifiability. Instead, the overall correlation of θ_i with θ can be inferred by the relative difference between IE and GE – though IE and GE are expressed in different units, as interactions can be repeated in the GE of two or more θ_i (Oakley & O'Hagan, 2004; Saltelli et al., 2006). Summarizing, both a low IE and a large IE to GE difference mean poor identifiability for a single θ_i, though *a priori* no fixed threshold – neither for IE, nor for GE minus IE – permits to distinguish whether θ_i should be considered as non-identifiable.

A maximum θ subset of $N' = 30$ and/or 400 simulations of $J(\theta)$ can be evaluated simultaneously with the GSA engine (Kennedy & Petropoulos, 2017). Therefore, to assess θ interactions when $N > 30$, a combination strategy was followed. Firstly, 30 θ_i were randomly selected and evaluated by GSA (i.e. GSA No. 1). From these θ, only those showing the smallest IE (e.g. < 1 %) were disregarded as non-identifiable, removed from the initial θ subset, and not used for further GSA. Importantly, these non-identifiable θ_i were fixed at their initial values [Table 4] for all subsequent model simulations, since non-identifiability implies that these θ can be fixed at any value within $p(\theta)$ (Dochain & Vanrolleghem, 2001; Guisasola et al., 2006). Then, θ_P and/or θ_B non-previously-assessed by GSA were combined with the non-removed θ subset, and a new GSA was performed (i.e. GSA No. 2). The GSA methodology was repeated until the last remaining θ subset was considered as 'potentially identifiable', θ'.

344 In total, seven GSA with different θ combinations were progressively performed [Table
345 5]. In this study, the only criterion for non-identifiability was assumed as IE ≤ 0.20 %,
346 which also coincided with a relatively low GE (i.e. < 4.5), though this conservative
347 criterion could be modified as mentioned in Section 3.1.1. To enhance the GSA
348 representativeness in presence of a high number of θ (i.e. $20 \leq N' \leq 30$) and/or wide
349 variability ranges (i.e. ± 50 %), each GSA was conducted in triplicate and the results
350 averaged. Finally, all $J(\theta)$ arrays used for GSA were searched for the minimum
351 observed value, $J_{min}(\theta)$ (i.e. $\geq J(\theta_{opt})$), to be subsequently used in ABC.
352

353 **2.3.5 Approximate Bayesian Computation**

354 The θ' posterior distribution, $p(\theta'|y)$, was assessed by ABC (Toni & Stumpf, 2010). In
355 short, multiple simulations were carried at different θ' combinations sampled by LHS,
356 whereas relatively high $J(\theta')$ values were discarded by a progressively stringent
357 criterion based in a tolerance coefficient, ε (i.e. > 1.0). In other words, only $J(\theta')$ -
358 $J_{min}(\theta') \leq \varepsilon$ were accepted for posterior evaluation: $p(\theta'|J(\theta') - J_{min}(\theta') \leq \varepsilon)$. With this
359 approach, θ' identifiability was further assessed by the convergence in the confidence
360 range.
361

362 In this study, ε was successively reduced from 2.50 to 1.05 (i.e. 2.50, 1.80, 1.30, 1.10
363 and 1.05). Within each explored $J(\theta') - J_{min}(\theta') \leq \varepsilon$ range, 400 simulations were used. θ'
364 were allowed to vary within the same range used for GSA [Table 4]. Meanwhile, the 5
365 to 95 % interquartile range of each θ' was used as confidence range, but also as a
366 criterion for identifiability/convergence. The posterior mean, median, mode, Kurtosis,

Skewness and correlation matrix were also evaluated, as described in Martin and Ayesa (2010).

2.3.6 Cross-Validation

Cross-validation assesses the model 'goodness of fitting' in experiments not used for calibration (Bennett et al., 2013). In this study, the θ' posterior mean was considered as θ_{opt}. Thus, θ_{opt} were used to simulate all batch experiments, including the three experimental conditions selected for cross-validation: Batch No. 2, 4 and 8 [Table 1].

3 RESULTS AND DISCUSSION

3.1 GSA – Selecting the Most Influencing Input Parameters for Calibration

3.1.1 Preliminary Identifiability Assessment

GSA results are summarized in Table 5. GSA was started with 30 θ_P and progressively led to only 14 θ': 13 θ_P (i.e. $K_{h,pr}$, $K_{h,ch,slow}$, $k_{m,fa}$, $k_{m,c5}$, $k_{m,c4}$, $k_{m,pro}$, $k_{m,ac}$, $k_{m,h2}$, k_d, $pH_{LL,ac}$, $f_{bu,su}$, $f_{ac,su}$, $f_{h2,su}$) and 1 θ_B (i.e. $X_{ac,Batch7}$). In this study, only the θ_i showing IE $\leq$ 0.20 % were fixed at their initial values [Table 4] to enhance the capabilities of GSA and ABC for calibrating structured AD models, as mentioned in Section 2.3.4. The overall $J(\theta)$ variance explained by the GSA engine was around 70 % in all cases, confirming the validity of this methodology to assess the most influential θ in the HS-AD model (Oakley & O'Hagan, 2004).

IE provides a relative measure of the θ_i practical identifiability, while a high θ_i correlation – high difference between IE and GE – suggests that θ_i cannot be

391 independently calibrated with the available set of experimental data (Saltelli et al.,
392 2006). As an example, GSA No. 1 showed that 40.7 % out of 72.4 % of the global *J(θ)*
393 variance was explained by adding up the IE of 30 θ_P [Table 5], while the remaining
394 31.7 % variance was explained by correlations among these. For example, $k_{m,c4}$
395 explained individually around 4.4 % of the global variance (i.e. IE), though showing GE
396 up to 17.9. This meant that the correlation of $k_{m,c4}$ with other θ was high, and any
397 improvement in *J(θ)* obtained by solely modifying $k_{m,c4}$ could be partially or totally
398 compensated by the modification of a correlated θ_i. In this line, the $k_{m,c4} \cdot f_{bu,bu}$
399 correlation in GSA No. 1 explained up to 2.8 % of the global variance (data not shown),
400 due to the influence of $f_{bu,su}$ in *J(θ)* (i.e. IE = 2.0 % and GE = 24.4) [Table 5].
401
402 In this study, θ_i were disregarded by a single and low-demanding criterion (i.e. IE ≤
403 0.20 %) [Table 5], since any chosen criterion for 'potential identifiability' would
404 influence the GSA results when N ≥ 30. Meanwhile, GSA also depends on N' (i.e. ≤ 30)
405 and/or the particular combination of θ_P and θ_B used. Thus, using a more demanding
406 identifiability criterion (e.g. IE ≤ 0.50 % instead of 0.20 %) might have led to discard θ_i
407 during preliminary GSA runs, which would be subsequently characterized as
408 'potentially identifiable'. For example, GSA No. 1 showed an IE = 0.22 % for $k_{m,c5}$,
409 whereas GSA No. 7 eventually showed an IE = 0.67 % [Table 5]. To enhance
410 identifiability, a strategy to reduce the gap between IE and GE for each θ_i is required
411 (Kennedy & Petropoulos, 2017). However, reducing the IE to GE gap in this study
412 would require to readapt the criterion used for 'potential identifiability'. One strategy
413 might consist on fixing those θ_i showing, for example, IE ≤ 0.30 % in GSA No. 7 (i.e.
414 $f_{ac,su}$), and then perform further rounds of GSA (i.e. GSA No. 8) until IE ~ GE for all θ_i.

With all the above, a second assessment for identifiability can be useful when using variance-based GSA for structured AD models. ABC is a well-suited tool in this regard, yielding also $p(\theta|y)$, in contrast to GSA. Importantly, both methodologies should yield equivalent results regarding the θ_i identifiability, though ABC is much computationally intensive than GSA, as explained in Section 3.2.1.

3.1.2. Importance of the $p(\theta)$ for Model Calibration

It must be noted that any $p(\theta)$ could be used to calibrate AD models, provided that θ do not contradict biochemical laws (e.g. $\theta_P \geq 0$ and $\theta_B \geq 0$) or disrupt mathematical resources (e.g. $pH_{UL,ac} > pH_{LL,ac}$) and the overall $p(\theta)$ range is as densely and homogeneously sampled as possible. On the other hand, the $p(\theta)$ distribution used (e.g. uniform, log-transformed uniform, normal) can be also crucial to determine $p(\theta|y)$ and the overall θ estimation.

In this study, using triplicates permitted to enhance the GSA representativeness (overall sampling) in presence of large N and $p(\theta)$ ranges. Meanwhile, a uniform distribution with mostly a 90 % modification was predefined for θ_P, whereas a log-transformed uniform distribution with a 50 % modification was allowed for θ_B [Table 4], as mentioned in Section 2.3.2. These specific $p(\theta)$ ranges were considered sufficiently wide for the objectives of this study, and were based mainly on experience and visual analysis of the overall model results. Particularly, the order of magnitude of many θ_P are relatively well characterized in literature according to their corresponding bio-physical-chemical meaning. Nonetheless, the order of magnitude of θ_B is highly unknown,

particularly after the inoculum centrifugation used in this study. Thus, using a uniform $p(\theta)$ permitted to emphasize the precision over punctual θ_P values within the $p(\theta_P)$ range, whereas the precision over the 'unknown' order of magnitude in the θ_B range was emphasized by using a log-transformed uniform distribution $p(log_{10}(\theta_B))$.

With all the above, using a different $p(\theta)$ range or distribution might alter the results of variance-based GSA and the overall calibration of structured AD models. For example, using considerably narrower $p(\theta_P)$ ranges in GSA No. 1 (i.e. $(1 - 0.3) \cdot \theta_{P,0} \leq \theta_P \leq (1 + 0.3) \cdot \theta_{P,0}$; *uniform* $p(\theta_P)$) resulted in some θ_P – which were highlighted as 'potentially identifiable' in this study – being disregarded as non-identifiable (e.g. $K_{h,pr}$ and $k_{m,c4}$), likely because part of their 'optimal' or 'sub-optimal' θ_P values were left outside the $p(\theta_P)$ range [Supplementary Information]. On the other hand, using wider ranges (i.e. $0.01 \cdot \theta_{P,0} \leq \theta_P \leq 3 \cdot \theta_{P,0}$; *uniform* $p(\theta_P)$), the results were not substantially different; i.e. only the $k_{m,c5}$ identifiability was additionally disregarded by GSA No. 1. However, using a log-transformed uniform distribution (i.e. $(1 + 0.5) \cdot log_{10}(\theta_{P,0}) \leq log_{10}(\theta_P) \leq (1 - 0.5) \cdot log10(\theta_{P,0})$; *uniform* $p(log_{10}(\theta_P))$) relatively altered the results of GSA No. 1; i.e. the order of magnitude of $k_{m,c5}$ and $k_{m,c4}$ was disregarded, while the order of magnitude of $K_{h,ch,slow}$ and $K_{S,Xh2}$ has was highlighted as highly important for the HS-AD model calibration. Therefore, for the correct calibration of structured AD models, both the $p(\theta)$ range and distribution should be set accordingly to all the prior information available for these θ, minimizing the $p(\theta)$ range explored alongside the number of simulations required for the objectives of the study.

3.1.3 Importance of the Available Data for Model Calibration

463 Provided the θ are structurally identifiable, practical identifiability relates to the quantity
464 as well as the quality (i.e. experimental errors and/or the sampling frequency) of the
465 experimental data available (Donoso-Bravo et al., 2011; Guisasola et al., 2006;
466 Nimmegeers et al., 2017; Rodriguez-Fernandez et al., 2006). Particularly, a reduced
467 number of experimental data associated to some model dynamics usually prevents
468 practical identifiability of the θ involved in these specific dynamics. For example, Y_b
469 might not be identifiable in AD models provided that the biomass concentration
470 dynamics were measured (Bernard et al., 2001).
471
472 In this study, the hydrolysis constant of readily-biodegradable carbohydrates ($K_{h,ch,fast}$)
473 and lipids ($K_{h,li}$), but also the maximum growth rate of sugar ($k_{m,su}$) and amino acid
474 ($k_{m,aa}$) degraders, showed a reduced influence in $J(\theta)$ by GSA. These results suggest that
475 either insufficient experimental data was available to calibrate $K_{h,ch,fast}$, $K_{h,li}$, $k_{m,su}$ and
476 $k_{m,aa}$, or that the biogas production in the HS-AD batch experiments [Table 1] was
477 mostly influenced by the VFA uptake – as the main limiting step. In the same line, due
478 to the Monod properties, k_m and K_S might be correlated when using batch experiments
479 for calibration (Dochain & Vanrolleghem, 2001; Flotats et al., 2010; Guisasola et al.,
480 2006). Nevertheless, GSA showed negligible influence for all K_S in this study, likely
481 due to using different batch experiments (i.e. ISR and TS) and/or a reduced number of
482 experimental data to obtain $J(\theta)$ [Equation 4].
483
484 The liquid-gas transfer coefficient (kLa) was also disregarded during the initial steps of
485 GSA (i.e. IE = 0.07 % and GE = 0.39) [Table 5]. The kLa coefficient is related to the
486 homogenization and mixing strategy, as well as other operational parameters in AD (e.g.

487 temperature and pH) (Batstone et al., 2002). In this study, all the HS-AD digesters were
488 manually shaken. However, increasing the TS content can hamper the liquid-gas
489 transfer mechanisms in HS-AD (Pastor-Poquet et al., 2019a). Therefore, a calibration
490 strategy should be specifically envisaged to correctly calibrate kLa (e.g. using different
491 stirring velocities/devices for mixing), since the presence of several θ in HS-AD models
492 can prevent identifiability of kLa with the reduced number of experimental data usually
493 available.
494
495 Importantly, both the NH_3 and H_2 inhibition parameters [Table 2] were shown as non-
496 identifiable in this study, despite the strong influence of these parameters to regulate the
497 biogas production in an ADM1-based model, as mentioned in Section 2.3.2. These
498 results were associated to the reduced TAN and VFA dynamics in the experimental data,
499 since only one single sacrifice experiment was available for calibration/validation.
500 Therefore, despite using different initial conditions (i.e. ISR and/or TS) for model
501 calibration, the NH_3 inhibition parameters in HS-AD of OFMSW cannot be assessed by
502 using traditional batch experiments, where only the biogas production and composition
503 are (usually) dynamically evaluated.
504
505 The above results condense the importance of an adequate sampling to enhance
506 identifiability in AD models, but also to test hypotheses regarding the effects of
507 inhibitory substances in HS-AD. Particularly, an extensive sampling for VFA, pH and
508 TAN at different operational times during batch experiments is required to identify
509 crucial parameters regarding the NH_3 inhibition in HS-AD of OFMSW. Therefore,
510 sacrifice experiments and/or any sampling technique for batch setups – allowing the

511 thorough characterization of the reactor content variables in dynamic mode – should be
512 recommended to calibrate structured HS-AD models using batch experiments. On the
513 other hand, including (semi-)continuous datasets when available might also alleviate
514 these identifiability issues during calibration (Bennett et al., 2013; Nimmegeers et al.,
515 2017).
516
517 **3.1.4 The Importance of Initial Conditions for Model Calibration**
518 Interestingly, all θ_B except $X_{ac,Batch7}$ were shown as non-identifiable in this study [Table
519 5]. The reason presumably lies on the high k_m of all microorganisms 'shading' the effect
520 of their initial concentration. For example, X_{pro} was associated to a maximum growth
521 rate ($k_{m,pro}$) around 10 d^{-1} [Table 4]. Thus, X_{pro} doubles within 1 h (i.e. $\frac{\log(2)}{k_m} =$
522 $\frac{\log(2)\cdot 24}{10} = 0.6\ h$), whereas the HS-AD batch experiments lasted considerably longer
523 than 20 days [Table 1].
524
525 X_{ac} and X_{h2} are important variables to avoid batch acidification during the initial 0 - 10
526 days of HS-AD simulations, due to the rapid changes occurring in the bio-physical-
527 chemistry during these days and the influence of these two microbial populations to
528 define the buffering capacity (Batstone et al., 2002; Capson-Tojo et al., 2017).
529 Nonetheless, these biomass concentrations were also rapidly disregarded by GSA in this
530 study [Tables 3 and 4], except the 'potential identifiability' of $X_{ac,Batch7}$ suggested by
531 GSA No. 7 which was likely explained by the influence of the order of magnitude of
532 this particular biomass content to regulate the risk of acidification of the most extreme
533 HS-AD condition in Experiment 7 (i.e. Batch No. 9, TS = 30 %) [Table 1].
534

With all the above, it is likely that only the initial biomass magnitude – not a precise value – was needed to calibrate the HS-AD model based on batch experiments. In other words, approximate biomass concentrations serve mainly to avoid acidification in HS-AD batch simulations, since these might not influence significantly the model calibration. The θ influence on $J(\theta)$ in this study was further assessed by ABC.

3.2 Parameter Optimization

3.2.1 Second Identifiability Assessment

Figure 1 shows $p(\theta'|y)$ using an $\varepsilon = 1.05$. The main statistics for these $p(\theta'|y)$ are summarized in Table 6, including the confidence ranges (i.e. 5 - 95 % interquartile range), since a reliable assessment of the θ confidence range is as important as the value of θ_{opt} themselves (Guisasola et al., 2006). The correlation matrix is included as Supplementary Information. Figure 2 shows the 5 - 95 % interquartile range *vs.* ε, since reducing progressively ε permitted to assess the convergence of the θ' posterior as second identifiability assessment.

Parameter identifiability is roughly associated to the 'sharpness' of the posterior distribution, $p(\theta|y)$ (Martin & Ayesa, 2010; Toni & Stumpf, 2010). In this line, $K_{h,pr}$, $K_{h,ch,slow}$, $k_{m,fa}$, $k_{m,c5}$, $k_{m,c4}$, $k_{m,ac}$, $pH_{LL,ac}$ and $f_{bu,su}$ showed relatively well-defined bell-shaped distributions by ABC, suggesting an adequate identifiability [Figure 1]. Meanwhile, $k_{m,pro}$, $k_{m,h2}$, k_d, $X_{ac,Batch7}$, $f_{ac,su}$ and $f_{h2,su}$ showed a more uniform-like distribution, suggesting a poorer identifiability. The substantial reduction observed in the interquartile range for $K_{h,pr}$, $K_{h,ch,slow}$, $k_{m,fa}$, $k_{m,c5}$, $k_{m,c4}$, $k_{m,ac}$, $pH_{LL,ac}$ and $f_{bu,su}$ (i.e. 60 - 80 %) corroborated their adequate identifiability in this study, in contrast to $k_{m,pro}$,

559 $k_{m,h2}$, k_d, $X_{ac,Batch7}$, $f_{ac,su}$ and $f_{h2,su}$ that showed a much constant interquartile range (i.e. ≤
560 50 % reduction) [Figure 2]. The poor practical identifiability of these last θ' is explained
561 by their high correlation with the rest of θ'. For example, the $f_{ac,su} \cdot f_{bu,su}$ correlation was -
562 0.82, while $k_{m,pro} \cdot k_d$ was 0.72 – data not shown. As suggested in Section 3.1.4, $X_{ac,Batch7}$
563 served mainly to counteract the potential acidification in Batch No. 9, since the poor
564 reduction in the interquartile range (i.e. 23 %) alongside the high correlation with other
565 θ' (i.e. $pH_{LL,ac} \cdot X_{ac,Batch7} = 0.24$) indicated that only an approximate biomass content is
566 needed to calibrate structured HS-AD models based on batch experiments.
567
568 As expected, ABC supported the identifiability assessment previously performed by
569 GSA. In particular, θ' showing IE < 1.5 % in GSA No. 7 (i.e. $k_{m,pro}$, $k_{m,h2}$, and $f_{ac,su}$)
570 [Table 5] were associated to a poor identifiability. However, some parameters showing
571 an IE ≥ 1.5 % in GSA No. 7 (i.e. k_d, $X_{ac,Batch7}$ and $f_{h2,su}$) were also indicated as non-
572 identifiable by ABC in contrast to GSA, suggesting that ABC was a more sensitive
573 methodology for parameter identifiability in this study. With all the above, a more
574 restrictive IE threshold (i.e. 0.50 % instead of 0.20 %) could have been used in further
575 GSA rounds, once fixing poorly-identifiable parameters to any value within the prior, as
576 mentioned in Section 3.1.1.
577
578 ABC is computationally intensive due to the high level of $J(\theta') - J_{min}(\theta') \leq \varepsilon$ rejection,
579 particularly when using highly-demanding ε (Filippi et al., 2013; Toni & Stumpf, 2010).
580 For example, the acceptance ratio was 0.129 when using ε = 1.80, meaning that only 1
581 out of 8 simulations was accepted for posterior evaluation, whereas the acceptance ratio
582 was 0.004 when using ε = 1.10 – data not shown. Thus, ABC is not recommended to

583 assess identifiability in complex models with a large number of θ (i.e. $N \geq 30$). Different
584 upgrades have been proposed to increase the ABC efficiency (Beaumont et al., 2009;
585 Filippi et al., 2013; Toni & Stumpf, 2010), though the evaluation of these upgrades for
586 calibrating structured AD models was out of the scope of this study. Conversely, the
587 GSA engine relies upon a Bayesian emulator to speed up the analysis of model outputs
588 (Kennedy & O'Hagan, 2001; Oakley & O'Hagan, 2004). Therefore, GSA can be an
589 adequate tool to reduce the global computation required for parameter optimization, by
590 preliminarily reducing the number of θ' to be further assessed by ABC as shown in this
591 study.
592
593 **3.2.2 Batch Simulations**
594 Using the θ' mean as θ_{opt} [Table 6] led to a good approximation of both the methane
595 production [Figure 3] and the rest of variables at the end of all batch experiments
596 [Figure 4] used either for calibration (i.e. Batch No. 1, 3, 5, 6, 7 and 9) or cross-
597 validation (i.e. Batch No. 2, 4 and 8) [Table 1]. Therefore, the θ' mean might be a good
598 approximation of θ_{opt}, particularly for those θ' where practical identifiability was likely
599 (i.e. $K_{h,pr}$, $K_{h,ch,slow}$, $k_{m,fa}$, $k_{m,c5}$, $k_{m,c4}$, $k_{m,ac}$, $pH_{LL,ac}$ and $f_{bu,su}$). Importantly, the HS-AD
600 model was able to capture particularly well the TS and TAN contents, but also VS (data
601 not shown), in all mono- and co-digestion experiments, confirming the suitability of the
602 hypotheses used for the model development (Pastor-Poquet et al., 2018).
603
604 Some disagreements were also observed between the simulations and the experimental
605 results. Particularly, the implementation of a reversible NH_3 inhibition function
606 [Equation 1] in all the VFA and H_2 degrading populations [Table 2] was unable to

607 capture the VFA accumulation at the end of HS-AD experiments [Figure 4]. As the
608 most noticeable example, calibration failed to represent the S_{bu} accumulation in Batch
609 No. 6 [Figure 4e], yielding also a slight miss-adjustment in the methane production
610 [Figure 3c]. More in general, S_{ac} and S_{bu} at the end of all experiments were poorly
611 represented [Figure 4], despite the butyrate ($k_{m,c4}$) and acetate ($k_{m,ac}$) growth rates were
612 adequately identified and the NH_3 inhibition upon the acetate uptake is a relatively well-
613 established strategy in structured AD models (Batstone et al., 2002).
614
615 Two main reasons might explain the VFA disagreement between the model simulations
616 and the experimental data available. The first reason relates to the relatively low amount
617 of experimental data hampering calibration, as mentioned in Section 3.1.3. In this line,
618 the NH_3 half-inhibition parameters in the VFA and/or H_2 uptakes ($K_{i,nh3}$) were
619 disregarded as unimportant by GSA to represent the experimental data [Table 5], mainly
620 because only Batch No. 1 contained the VFA, pH and TAN dynamics. The second
621 reason relates to the poor suitability of the reversible non-competitive NH_3 inhibition
622 function [Equation 1] to explain the VFA accumulation in HS-AD simulations, as
623 discussed in next section.
624
625 **3.3 Main Effects of Increasing the TS Content in HS-AD of OFMSW**
626 In this study, calibration/cross-validation served to further test the hypotheses used for
627 model construction (e.g. mass balances), particularly regarding the TS and VS
628 simulation. Noteworthy, the correct simulation of TS is crucial in HS-AD, as TS
629 determines the apparent concentration of soluble compounds subsequently affecting all
630 the HS-AD bio-physical-chemical dynamics (Pastor-Poquet et al., 2019b). For example,

631 TS = 20 % supposes approximately 20 % higher apparent concentrations (i.e. kmol/kg
632 H_2O) regarding the corresponding global concentrations (i.e. kmol/kg).
633
634 The HS-AD model was also calibrated/validated to assess the effects of increasing TS
635 upon the NH_3 inhibition in HS-AD. Specifically, a high solute content – potentially
636 associated to a high TS – exacerbates the solution 'non-ideality', affecting all the HS-
637 AD dynamics (e.g. pH, NH_3 concentration, CO_2 transfer) (Pastor-Poquet et al., 2019b).
638 More in detail, 'non-ideality' can lower S_{nh3}, serving as a potential source of NH_3
639 inhibition abatement in HS-AD of OFMSW. In this study, *I* ranged from 0.22 to 0.93 M
640 [Figure 4c], emphasizing the need for an adequate 'non-ideal' bio-physical-chemical
641 approach (Hafner & Bisogni, 2009; Solon et al., 2015). Importantly, despite the high *I*
642 observed, S_{nh3} reached up to 0.13 mol N/kg in this study [Figure 4d] – equivalent to
643 0.16 mol N/kg H_2O (i.e. 2.3 g N/L). These S_{nh3} were considerably high, since reactors
644 operated at $S_{nh3} \geq 1.0$ g N/L usually show an inefficient VFA conversion (Rajagopal et
645 al., 2013).
646
647 The inefficient VFA conversion in HS-AD experiments was not well simulated by the
648 reversible NH_3 inhibition function, as mentioned in Section 3.2.2. To understand the
649 poor VFA simulation, it is necessary to consider the relatively flat inhibition described
650 by Equation 1 but also the COD fluxes in the HS-AD model. Briefly, I_{nh3} is 0.50 when
651 $S_{nh3,App} = K_{i,Snh3}$, whereas I_{nh3} is 0.33 when $S_{nh3,App} = 2 \cdot K_{i,Snh3}$ [Equation 1]. In other
652 words, a non-competitive reversible inhibition by NH_3 might be far too 'blunt' to
653 describe the actual effect of NH_3 upon the anaerobic biomass (Astals et al., 2018). On
654 the other hand, due to the COD fractioning used in this study, approximately 54 % of

655 the COD from S_{su} [Table 6] and 26 % of the COD from S_{aa} flowed through the butyrate
656 pathway, whereas up to 80 % of the COD either from S_{su}, S_{aa} and/or long-chain fatty
657 acids (S_{fa}) flowed through the acetate pathway (Batstone et al., 2002). Meanwhile, a
658 considerable proportion of the initially biodegradable COD (i.e. 75 - 85 %) was
659 assigned to $X_{ch} + S_{su} + X_{pr} + S_{aa}$ [Table 3].
660
661 With all the above, the 'blunt' definition of the NH_3 inhibition function, alongside the
662 high COD flowing through the butyrate and acetate pathways, presumably favored the
663 X_{bu} and X_{ac} growth even at considerably high S_{nh3} (i.e. up to 2.3 g N/L) during
664 simulations. Summarizing, the high substrate content counterbalanced the effect of the
665 NH_3 inhibition, preventing the correct simulation of S_{bu} and S_{ac} accumulation at the end
666 of the HS-AD experiments. Therefore, the reversible non-competitive NH_3 inhibition
667 function [Equation 1] in the VFA and/or H_2 uptakes [Table 2] requires further testing to
668 represent the VFA accumulation observed in HS-AD of OFMSW. To this particular aim,
669 using extensive data regarding the VFA, pH and TAN dynamics in HS-AD simulations
670 is strongly recommended.
671
672 To end up, the HS-AD model (Pastor-Poquet et al., 2018) is a suitable platform to
673 understand the inner mechanisms of HS-AD, whereas further model developments
674 and/or model configurations (i.e. inhibition functions) should be also tested to enhance
675 our understanding about the VFA accumulation within HS-AD of OFMSW. Similarly,
676 additional experimental data is needed to thoroughly understand the role of NH_3
677 inhibition in HS-AD simulations. Specifically, extensive data regarding the main
678 species driving 'non-ideality' (i.e. VFA, pH, TAN) and/or further bio-physical-chemical

679 mechanisms (i.e. precipitation) in HS-AD seem to be crucial, due to the outstanding
680 importance of 'non-ideality' for the biochemical parameter optimization (Pastor-Poquet
681 et al., 2019b). In this scheme, the relatively simple calibration/validation methodology
682 presented in this study can serve to test the θ practical identifiability and confidence
683 ranges in presence of any set of experimental data and/or HS-AD model structure.
684
685
686 **4 CONCLUSIONS**
687 Nine different batch conditions were used to calibrate and cross-validate the HS-AD
688 model. For parameter optimization, variance-based GSA in tandem with ABC served to
689 evaluate the practical identifiability of 35 θ_P and 32 θ_B. Among all these, mostly 8 θ_P
690 were correctly identified with the available data, as corroborated by the convergence of
691 $p(\theta|y)$. The study also showed that HS-AD may be operated at $S_{nh3} \geq 2.3$ g N/L and $I \geq$
692 0.9 M, whereas a reversible non-competitive NH_3 inhibition function was not able to
693 explain the VFA accumulation in HS-AD of OFMSW. Therefore, further datasets about
694 the VFA, pH and TAN dynamics are required to enhance the θ practical identifiability,
695 whereas further model configurations should be tested to enhance the simulation of NH_3
696 inhibition in HS-AD.
697
698
699 **Acknowledgements**
700 This project has received funding from the European Union's Horizon 2020 research
701 and innovation programme under the Marie Sklodowska-Curie grant agreement No.

643071. Angela Andreella is gratefully acknowledged for revising all the statistical concepts.

REFERENCES

Astals, S., Peces, M., Batstone, D.J., Jensen, P.D., Tait, S. 2018. Characterising and modelling free ammonia and ammonium inhibition in anaerobic systems. *Water Res.*, **143**, 127-135.

Batstone, D.J., Keller, J., Angelidaki, I., Kalyuzhnyi, S.V., Pavlostathis, S.G., Rozzi, A., . . . Vavilin, V.A. 2002. The IWA Anaerobic Digestion Model No. 1 (ADM1). *Water Sci. Technol.*, **45**(10), 65-73.

Beaumont, M.A., Cornuet, J.-M., Marin, J.-M., Robert, C.P. 2009. Adaptive approximate Bayesian computation. *Biometrika*, **96**(4), 983-990.

Bennett, N.D., Croke, B.F.W., Guariso, G., Guillaume, J.H.A., Hamilton, S.H., Jakeman, A.J., . . . Andreassian, V. 2013. Characterising performance of environmental models. *Environ. Model. Software*, **40**, 1-20.

Bernard, O., Hadj-Sadok, Z., Dochain, D., Genovesi, A., Steyer, J.P. 2001. Dynamical model development and parameter identification for an anaerobic wastewater treatment process. *Biotechnol. Bioeng.*, **75**, 424-438.

Capson-Tojo, G., Trably, E., Rouez, M., Crest, M., Steyer, J.P., Delgenès, J.P., Escudié, R. 2017. Dry anaerobic digestion of food waste and cardboard at different substrate loads, solid contents and co-digestion proportions. *Bioresour. Technol.*, **233**, 166-175.

Dochain, D., Vanrolleghem, P. 2001. *Dynamical Modelling and Estimation in Wastewater Treatment Processes*. IWA Publishing, London, UK.

Donoso-Bravo, A., Mailier, J., Martin, C., Rodríguez, J., Aceves-Lara, C.A., Vande Wouwer, A. 2011. Model selection, identification and validation in anaerobic digestion: A review. *Water Res.*, **45**(17), 5347-5364.

Filippi, S., Barnes, C.P., Cornebise, J., Stumpf, M.P. 2013. On optimality of kernels for approximate Bayesian computation using sequential Monte Carlo. *Stat. Appl. Genet. Mol. Biol.*, **12**(1), 87–107.

Flotats, X., Ahring, B.K., Angelidaki, I. 2003. Parameter identification of thermophilic anaerobic degradation of valerate. *Appl. Biochem. Biotechnol.*, **109**(1-3), 47-62.

Flotats, X., Palatsi, J., Fernandez, B., Colomer, M.A., Illa, J. 2010. Identifying anaerobic digestion models using simultaneous batch experiments. *Environ. Engineer. Manag. J.*, **9**(3), 313-318.

Garcia-Gen, S., Sousbie, P., Rangaraj, G., Lema, J.M., Rodriguez, J., Steyer, J.P., Torrijos, M. 2015. Kinetic modelling of anaerobic hydrolysis of solid wastes, including disintegration processes. *Waste Manage.*, **35**, 96-104.

744 Guisasola, A., Baeza, J.A., Carrera, J., Sin, G., Vanrolleghem, P.A., Lafuente, J. 2006.
745 The influence of experimental data quality and quantity on parameter estimation
746 accuracy: Andrews inhibition model as a case study. *Educ. Chem. Eng.*, **1**(1),
747 139-145.
748 Hafner, S.D., Bisogni, J.J. 2009. Modeling of ammonia speciation in anaerobic
749 digesters. *Water Res.*, **43**(17), 4105-4114.
750 Kennedy, M.C., O'Hagan, A. 2001. Bayesian calibration of computer models. *J. Roy.*
751 *Stat. Soc. Ser. B. (Stat. Method.)*, **63**(3), 425-464.
752 Kennedy, M.C., Petropoulos, G.P. 2017. GEM-SA: The gaussian emulation machine for
753 sensitivity analysis. in: *Sensitivity Analysis in Earth Observation Modelling*,
754 (Ed.) G.P. Petropoulos, Elsevier. Amsterdam, Netherlands.
755 Martin, C., Ayesa, E. 2010. An Integrated Monte Carlo Methodology for the calibration
756 of water quality models. *Ecol. Model.*, **221**(22), 2656-2667.
757 Nimmegeers, P., Lauwers, J., Telen, D., Logist, F., Impe, J.V. 2017. Identifiability of
758 large-scale non-linear dynamic network models applied to the ADM1-case
759 study. *Math. Biosci.*, **288**, 21-34.
760 Nott, D.J., Marshall, L., Brown, J. 2012. Generalized likelihood uncertainty estimation
761 (GLUE) and approximate Bayesian computation: What's the connection? *Water*
762 *Resour. Res.*, **48**(12).
763 Oakley, J.E., O'Hagan, A. 2004. Probabilistic sensitivity of complex models: A
764 Bayesian approach. *J. Roy. Stat. Soc. Ser. B. (Stat. Method.)*, **66**(3), 751-769.
765 Pastor-Poquet, V., Papirio, S., Steyer, J.-P., Trably, E., Escudié, R., Esposito, G. 2018.
766 High-solids anaerobic digestion model for homogenized reactors. *Water Res.*,
767 **142**, 501-511.
768 Pastor-Poquet, V., Papirio, S., Trably, E., Rintala, J., Escudié, R., Esposito, G. 2019a.
769 High-Solids Anaerobic Digestion requires a tradeoff between Total Solids,
770 Inoculum-to-Substrate Ratio and Ammonia Inhibition. *Int. J. Environ. Sci.*
771 *Technol.*, 1-15.
772 Pastor-Poquet, V., Papirio, S., Steyer, J.-P., Trably, E., Escudié, R., Esposito, G. 2019b.
773 Modelling Non-Ideal Bio-Physical-Chemical Effects on High-Solids Anaerobic
774 Digestion of the Organic Fraction of Municipal Solid Waste. *J. Environ.*
775 *Manage.*, **238**, 408-419.
776 Rajagopal, R., Masse, D.I., Singh, G. 2013. A critical review on inhibition of anaerobic
777 digestion process by excess ammonia. *Bioresour. Technol.*, **143**, 632-641.
778 Ratto, M., Tarantola, S., Saltelli, A. 2001. Sensitivity analysis in model calibration:
779 GSA-GLUE approach. *Comput. Phys. Commun.*, **136**, 212-224.
780 Rodriguez-Fernandez, M., Egea, J.A., Banga, J.R. 2006. Novel metaheuristic for
781 parameter estimation in nonlinear dynamic biological systems. *BMC*
782 *Bioinformatics*, **7**, 483.
783 Saltelli, A., Ratto, M., Tarantola, S., Campolongo, F. 2006. Sensitivity analysis
784 practices: Strategies for model-based inference. *Reliab. Eng. Syst. Saf.*, **91**(10-
785 11), 1109-1125.
786 Solon, K., Flores-Alsina, X., Mbamba, C.K., Volcke, E.I., Tait, S., Batstone, D., . . .
787 Jeppsson, U. 2015. Effects of ionic strength and ion pairing on (plant-wide)
788 modelling of anaerobic digestion. *Water Res.*, **70**, 235-245.
789 Toni, T., Stumpf, M.P. 2010. Simulation-based model selection for dynamical systems
790 in systems and population biology. *Bioinformatics*, **26**(1), 104-110.
791

792 **TABLE CAPTIONS**

793 **Table 1**. Batch experiments and initial conditions used for HS-AD model calibration
794 and cross-validation
795 **Table 2**. Biochemical rates used for the HS-AD model in this study
796 **Table 3**. Initial conditions used for all batch simulations in this study
797 **Table 4**. Main input parameters (θ) used for global sensitivity analysis (GSA), including
798 the initial values, lower and upper thresholds
799 **Table 5**. Global sensitivity analysis (GSA) of input parameters (θ): Individual (IE) and
800 global (GE) effects upon the objective function, $J(\theta)$, variance
801 **Table 6**. Calibration of potentially-identifiable input parameters (θ'): Prior and posterior
802 distributions
803
804

805 **FIGURE CAPTIONS**
806
807 **Figure 1**. Posterior parameter distribution using 400 simulations and $\varepsilon = 1.05$
808 **Figure 2**. Interquartile range (percentiles 5 to 95 %) of the posterior parameter
809 distribution using $\varepsilon \geq 1.05$ and $\varepsilon \leq 2.50$
810 **Figure 3**. Methane production with mono-digestion of dried OFMSW at a) ISR = 1.00;
811 b) ISR = 1.50; and c) ISR = 1.00; and co-digestion of dried OFMSW and sawdust at d)
812 ISR = 0.16. Dots represent experimental data, while lines represent simulated values.
813 **Figure 4**. Main variables at the end of the four batch experiments: a) Total solids (TS);
814 b) total ammonia nitrogen (TAN, S_{in}); c) ionic strength (I); d) free ammonia nitrogen
815 (NH_3, S_{nh3}); e) acetic acid (S_{ac}); f) propionic acid (S_{pro}); g) butyric acid (S_{bu}); and h)
816 valeric acid (S_{va}). Crosses represent experimental data, while geometries represent
817 simulated values
818
819

Table 1. Batch experiments and initial conditions used for HS-AD model calibration and cross-validation

Substrate	Exp. No.	Batch No.	ISR (g VS/g VS)	Initial TS (%)	No. Replicates	Design Volume (mL)	Exp. Time (days)	Calibration or Validation
OFMSW	**1**	1	1.00	15.0	15	280	92	C
	2	2	1.50	10.8	3	160	100	V
		3		13.4	3			C
		4		16.4	3			V
		5		19.6	3			C
	3	6	0.50	28.3	2	280	99	C
OFMSW + Sawdust	**4**	7	0.16	10.0	3	280	284	C
		8		15.0	2			V
		9		30.2	1			C

Table 2. Biochemical rates used for the HS-AD model in this study

Process	Rate (r_j, kgCOD m^{-3} d^{-1})
Hydrolysis of Fast Biodegradable Carbohydrates	$k_{h,ch,fast} \cdot X_{ch,fast}$
Hydrolysis of Slow Biodegradable Carbohydrates	$k_{h,ch,slow} \cdot X_{ch,slow}$
Hydrolysis of Proteins	$k_{h,pr} \cdot X_{pr}$
Hydrolysis of Lipids	$k_{h,li} \cdot X_{li}$
Sugars Uptake	$k_{m,su} \cdot S_{su,App}/(K_{S,Xsu}+S_{su,App}) \cdot X_{su} \cdot I_{pH} \cdot I_{in}$
Aminoacids Uptake	$k_{m,aa} \cdot S_{aa,App}/(K_{S,Xaa}+S_{aa,App}) \cdot X_{aa} \cdot I_{pH} \cdot I_{in}$
LCFA Uptake	$k_{m,fa} \cdot S_{fa}/(K_{S,Xfa}+S_{fa}) \cdot X_{fa} \cdot I_{pH} \cdot I_{in} \cdot I_{h2}$
Valerate Uptake	$k_{m,c5} \cdot S_{va,App}/(K_{S,Xc5}+S_{va,App}) \cdot X_{c5} \cdot I_{pH} \cdot I_{in} \cdot I_{h2} \cdot I_{nh3}$
Butyrate Uptake	$k_{m,c4} \cdot S_{bu,App}/(K_{S,Xc4}+S_{bu,App}) \cdot X_{c4} \cdot I_{pH} \cdot I_{in} \cdot I_{h2} \cdot I_{nh3}$
Propionate Uptake	$k_{m,pro} \cdot S_{pro,App}/(K_{S,Xpro}+S_{pro,App}) \cdot X_{pro} \cdot I_{pH} \cdot I_{in} \cdot I_{h2} \cdot I_{nh3}$
Acetate Uptake	$k_{m,ac} \cdot S_{ac,App}/(K_{S,Xac}+S_{ac,App}) \cdot X_{ac} \cdot I_{pH} \cdot I_{in} \cdot I_{nh3}$
Hydrogen Uptake	$k_{m,h2} \cdot S_{h2,App}/(K_{S,Xh2}+S_{h2,App}) \cdot X_{h2} \cdot I_{pH} \cdot I_{in} \cdot I_{nh3}$
Sugar Degraders Decay	$k_d \cdot X_{su}$
Aminoacids Degraders Decay	$k_d \cdot X_{aa}$
LCFA Degraders Decay	$k_d \cdot X_{fa}$
Valerate Degraders Decay	$k_d \cdot X_{c5}$
Butyrate Degraders Decay	$k_d \cdot X_{c4}$
Propionate Degraders Decay	$k_d \cdot X_{pro}$
Acetate Degraders Decay	$k_d \cdot X_{ac}$
Hydrogen Degraders Decay	$k_d \cdot X_{h2}$

with
$I_{in} = S_{in,App}/(K_{i,Sin} + S_{in,App})$
$I_{h2} = K_{i,Sh2}/(K_{i,Sh2} + S_{h2,App})$
$I_{pH} = K_{pH}\text{^}N_{pH}/(K_{pH}\text{^}N_{pH} + S_{h+}\text{^}N_{pH})$
$I_{nh3} = K_{i,Snh3}/(K_{i,Snh3} + S_{nh3,App})$

Table 3. Initial conditions used for all batch simulations in this study

Name	Mono-digestion						Co-digestion			Units
	ISR = 1.00	ISR = 1.50				ISR = 0.50	ISR = 0.16			
	TS=15.0%	TS=9.5%	TS=13.5%	TS=16.5%	TS=19.4%	TS=28.3%	TS=10.0%	TS=15.0%	TS=30.2%	
S_{su}	9.761	6.920	8.776	10.861	13.245	6.201	1.800	2.779	6.496	kg COD m^{-3}
S_{aa}	3.187	5.856	7.346	9.099	11.201	7.679	0.972	1.503	3.571	kg COD m^{-3}
S_{fa}	2.610	1.656	2.186	2.702	3.184	1.467	0.377	0.579	1.300	kg COD m^{-3}
S_{va}	0.791	1.015	1.282	1.582	1.936	1.061	1.467	2.269	5.314	kg COD m^{-3}
S_{bu}	0.500	0.195	0.244	0.302	0.370	1.518	0.230	0.355	0.831	kg COD m^{-3}
S_{pro}	2.059	0.877	1.109	1.368	1.674	2.565	1.367	2.115	4.952	kg COD m^{-3}
S_{ac}	0.103	0.035	0.044	0.054	0.066	0.871	0.058	0.090	0.210	kg COD m^{-3}
S_{h2}	1.00E-08	1.00E-08	1.00E-08	1.00E-08	1.00E-08	1.00E-08	1.00E-08	1.00E-08	1.00E-08	kg COD m^{-3}
S_{ch4}	1.00E-08	1.00E-08	1.00E-08	1.00E-08	1.00E-08	1.00E-08	1.00E-08	1.00E-08	1.00E-08	kg COD m^{-3}
S_{ic}	0.029	0.014	0.017	0.021	0.026	0.037	0.008	0.013	0.030	kmol C m^{-3}
S_{in}	0.186	0.125	0.157	0.194	0.238	0.229	0.033	0.051	0.120	kmol N m^{-3}
S_{i}	1.00E-08	1.00E-08	1.00E-08	1.00E-08	1.00E-08	1.00E-08	1.00E-08	1.00E-08	1.00E-08	kg COD m^{-3}
$S_{i,subs}$	34.706	29.233	37.076	45.883	55.954	90.351	27.565	42.559	99.486	kgCOD m^{-3}
$X_{ch,fast}$	29.283	13.840	17.553	21.722	26.490	31.003	5.400	8.337	19.489	kg COD m^{-3}
$X_{ch,slow}$	-	-	-	-	-	-	27.360	42.242	98.743	kg COD m^{-3}
X_{pr}	28.680	11.713	14.692	18.197	22.402	38.393	5.834	9.016	21.425	kg COD m^{-3}
X_{g}	18.271	3.312	4.373	5.405	6.367	5.866	2.637	4.053	9.102	kg COD m^{-3}
X_{su} (*)	0.050	0.050	0.063	0.078	0.095	0.150	0.005	0.008	0.018	kg COD m^{-3}
X_{aa} (*)	0.050	0.050	0.063	0.078	0.095	0.060	0.005	0.008	0.018	kg COD m^{-3}
X_{fa} (*)	0.010	0.020	0.025	0.031	0.038	0.030	0.001	0.001	0.002	kg COD m^{-3}
X_{c5} (*)	0.005	0.010	0.013	0.016	0.019	0.030	0.001	0.001	0.002	kgCOD m^{-3}
X_{c4} (*)	0.001	0.050	0.063	0.078	0.095	0.030	0.001	0.001	0.002	kg COD m^{-3}
X_{pro} (*)	0.005	0.020	0.025	0.031	0.038	0.030	0.001	0.001	0.003	kg COD m^{-3}
X_{ac} (*)	0.024	0.150	0.190	0.234	0.286	0.100	0.003**	0.005	0.011	kg COD m^{-3}
X_{h2} (*)	0.050	0.200	0.253	0.312	0.382	0.090	0.003	0.005	0.011	kg COD m^{-3}
X_{i}	1.00E-08	1.00E-08	1.00E-08	1.00E-08	1.00E-08	1.00E-08	1.00E-08	1.00E-08	1.00E-08	kg COD m^{-3}
$X_{i,subs}$	86.765	73.083	92.689	114.706	139.885	225.877	68.914	106.398	248.714	kg COD m^{-3}
S_{cat}	0.100	0.060	0.075	0.091	0.109	0.166	0.040	0.059	0.120	kmoleq m^{-3}
S_{an}	0.051	0.040	0.050	0.060	0.073	0.069	0.020	0.030	0.060	kmoleq m^{-3}
M_{Global}	37.12	29.92	24.02	19.80	16.47	23.45	138.23	93.13	46.13	g
ρ_{Global}	1078	1059	1075	1093	1113	1128	1088	1134	1316	kg m^{-3}
TS	15.0	10.8	13.4	16.4	19.6	28.3	10.0	15.0	30.2	%
VS	12.4	9.1	11.4	13.9	16.6	24.0	9.6	14.2	28.6	%
$N_{i,subs}$	0.0010	0.0012	0.0012	0.0012	0.0012	0.0010	0.0004	0.0004	0.0004	kmol N kg COD^{-1}
$V_{Reactor}$	280	160	160	160	160	280	160	160	160	mL

** These values were assessed by Global Sensitivity Analysis (GSA). ** This value was also assessed by Approximate Bayesian Computation (ABC). The inoculum-to-substrate ratio (ISR) is expressed in g VS/g VS*

Table 4. Main input parameters (θ) used for global sensitivity analysis (GSA), including the initial values, lower and upper thresholds

Model Parameter	Units	ADM1	Initial Value	Lower Threshold	Upper Threshold	Initial Concentration	Units	Initial Value*	Lower Threshold*	Upper Threshold*
$K_{h,ch,fast}$	d^{-1}	10	0.120	0.012	0.228	$X_{su,Batch1}$	kg COD m^{-3}	-1.301	-1.952	-0.651
$K_{h,pr}$	d^{-1}	10	0.050	0.005	0.095	$X_{su,Batch2}$	kg COD m^{-3}	-1.301	-1.952	-0.651
$K_{h,li}$	d^{-1}	10	0.080	0.008	0.152	$X_{su,Batch6}$	kg COD m^{-3}	-0.824	-1.236	-0.412
$K_{h,ch,slow}$	d^{-1}	-	0.012	0.001	0.023	$X_{su,Batch7}$	kg COD m^{-3}	-2.301	-3.452	-1.151
$k_{m,su}$	d^{-1}	70	70	7	133	$X_{aa,Batch1}$	kg COD m^{-3}	-1.301	-1.952	-0.651
$k_{m,aa}$	d^{-1}	70	70	7	133	$X_{aa,Batch2}$	kg COD m^{-3}	-1.301	-1.952	-0.651
$k_{m,fa}$	d^{-1}	10	10	1	19	$X_{aa,Batch6}$	kg COD m^{-3}	-1.222	-1.833	-0.611
$k_{m,c5}$	d^{-1}	30	8	1	15	$X_{aa,Batch7}$	kg COD m^{-3}	-2.301	-3.452	-1.151
$k_{m,c4}$	d^{-1}	30	13	1	25	$X_{fa,Batch1}$	kg COD m^{-3}	-2.000	-3.000	-1.000
$k_{m,pro}$	d^{-1}	20	10	1	19	$X_{fa,Batch2}$	kg COD m^{-3}	-1.699	-2.548	-0.849
$k_{m,ac}$	d^{-1}	16	16	2	30	$X_{fa,Batch6}$	kg COD m^{-3}	-1.523	-2.284	-0.761
$k_{m,h2}$	d^{-1}	35	20	2	38	$X_{fa,Batch7}$	kg COD m^{-3}	-3.301	-4.952	-1.651
k_{d}	d^{-1}	0.040	0.040	0.004	0.076	$X_{c5,Batch1}$	kg COD m^{-3}	-2.301	-3.452	-1.151
$K_{S,Xsu}$	kg COD m^{-3}	1.00	1.00	0.1	1.9	$X_{c5,Batch2}$	kg COD m^{-3}	-2.000	-3.000	-1.000
$K_{S,Xaa}$	kg COD m^{-3}	0.30	0.30	0.03	0.57	$X_{c5,Batch6}$	kg COD m^{-3}	-1.523	-2.284	-0.761
$K_{S,Xfa}$	kg COD m^{-3}	0.40	0.40	0.04	0.76	$X_{c5,Batch7}$	kg COD m^{-3}	-3.222	-4.833	-1.611
$K_{S,Xc5}$	kg COD m^{-3}	0.40	0.40	0.04	0.76	$X_{c4,Batch1}$	kg COD m^{-3}	-3.000	-4.500	-1.500
$K_{S,Xc4}$	kg COD m^{-3}	0.40	0.40	0.04	0.76	$X_{c4,Batch2}$	kg COD m^{-3}	-1.301	-1.952	-0.651
$K_{S,Xpro}$	kg COD m^{-3}	0.30	0.30	0.03	0.57	$X_{c4,Batch6}$	kg COD m^{-3}	-1.523	-2.284	-0.761
$K_{S,Xac}$	kg COD m^{-3}	0.30	0.30	0.03	0.57	$X_{c4,Batch7}$	kg COD m^{-3}	-3.222	-4.833	-1.611
$K_{S,Xh2}$	kg COD m^{-3}	5.00E-05	5.00E-05	0.000005	0.000095	$X_{pro,Batch1}$	kg COD m^{-3}	-2.301	-3.452	-1.151
$pH_{LL,ac}$	-	6.00	5.80	5.00	6.90	$X_{pro,Batch2}$	kg COD m^{-3}	-1.699	-2.548	-0.849
$K_{i,Snh3,Xc5}$	kmol N m^{-3}	-	0.0070	0.0007	0.0133	$X_{pro,Batch6}$	kg COD m^{-3}	-1.523	-2.284	-0.761
$K_{i,Snh3,Xc4}$	kmol N m^{-3}	-	0.0100	0.0010	0.0190	$X_{pro,Batch7}$	kg COD m^{-3}	-3.097	-4.645	-1.548
$K_{i,Snh3,Xpro}$	kmol N m^{-3}	-	0.0100	0.0010	0.0190	$X_{ac,Batch1}$	kg COD m^{-3}	-1.620	-2.430	-0.810
$K_{i,Snh3,Xac}$	kmol N m^{-3}	0.0110	0.0040	0.0004	0.0076	$X_{ac,Batch2}$	kg COD m^{-3}	-0.824	-1.236	-0.412
$K_{i,Snh3,Xh2}$	kmol N m^{-3}	-	0.0150	0.0015	0.0285	$X_{ac,Batch6}$	kg COD m^{-3}	-1.000	-1.500	-0.500
$f_{bu,su}$	kg COD kg COD^{-1}	0.130	0.500	0.050	0.950	$X_{ac,Batch7}$	kg COD m^{-3}	-2.523	-3.784	-1.261
$f_{ac,su}$	kg COD kg COD^{-1}	0.270	0.290	0.029	0.551	$X_{h2,Batch1}$	kg COD m^{-3}	-1.301	-1.952	-0.651
$f_{h2,su}$	kg COD kg COD^{-1}	0.190	0.100	0.010	0.190	$X_{h2,Batch2}$	kg COD m^{-3}	-0.699	-1.048	-0.349
$K_{i,Sh2,Xfa}$	kg COD m^{-3}	3.00E-05	1.00E-05	1.00E-06	1.90E-05	$X_{h2,Batch6}$	kg COD m^{-3}	-1.046	-1.569	-0.523
$K_{i,Sh2,Xc5}$	kg COD m^{-3}	3.00E-05	3.00E-05	3.00E-06	5.70E-05	$X_{h2,Batch7}$	kg COD m^{-3}	-2.523	-3.784	-1.261
$K_{i,Sh2,Xc4}$	kg COD m^{-3}	3.00E-05	3.00E-05	3.00E-06	5.70E-05	-	-	-	-	
$K_{i,Sh2,Xpro}$	kg COD m^{-3}	1.00E-05	1.00E-05	1.00E-06	1.90E-05	-	-	-	-	
$k_{L}a$	d^{-1}	200	200	20	380	-	-	-	-	

** Logarithm-transformed: $log_{10}(\theta_B)$*

Table 5. Global sensitivity analysis (GSA) of input parameters (θ): Individual (IE) and global (GE) effects upon the objective function, $J(\theta)$, variance

GSA No.1			GSA No.2			GSA No.3			GSA No.4			GSA No.5			GSA No.6			GSA No.7		
θ	IE (%)	GE	θ	IE (%)	GE	θ	IE (%)	GE	θ	IE (%)	GE	θ	IE (%)	GE	θ	IE (%)	GE	θ	IE (%)	GE
$K_{h,ch,fast}$	0.08	0.63	$K_{h,pr}$	1.75	5.23	$K_{h,pr}$	2.75	8.62	$K_{h,pr}$	2.21	7.33	$K_{h,pr}$	1.01	5.42	$K_{h,pr}$	2.00	10.44	$K_{h,pr}$	1.97	7.72
$K_{h,pr}$	2.01	7.56	$K_{h,li}$	0.25	0.69	$K_{h,li}$	0.26	2.54	$K_{h,li}$	0.11	2.85	$K_{h,ch,slow}$	4.28	14.61	$K_{h,ch,slow}$	4.07	14.47	$K_{h,ch,slow}$	4.43	17.86
$K_{h,li}$	0.29	2.07	$K_{h,ch,slow}$	5.87	16.21	$K_{h,ch,slow}$	5.83	14.32	$K_{h,ch,slow}$	5.22	16.59	$k_{m,fa}$	0.46	4.14	$k_{m,fa}$	1.15	5.66	$k_{m,fa}$	1.11	8.95
$K_{h,ch,slow}$	6.45	17.27	$k_{m,aa}$	0.07	0.43	$k_{m,fa}$	1.21	7.25	$k_{m,fa}$	0.56	4.81	$k_{m,c5}$	0.22	1.63	$k_{m,c5}$	1.59	8.34	$k_{m,c5}$	0.67	5.72
$k_{m,su}$	0.16	3.82	$k_{m,fa}$	0.81	5.97	$k_{m,c5}$	0.80	3.12	$k_{m,c5}$	0.73	3.31	$k_{m,c4}$	1.38	11.18	$k_{m,c4}$	1.50	13.79	$k_{m,c4}$	2.39	15.94
$k_{m,aa}$	0.53	2.43	$k_{m,c5}$	0.33	1.49	$k_{m,c4}$	2.23	17.17	$k_{m,c4}$	2.47	19.12	$k_{m,pro}$	1.77	8.66	$k_{m,pro}$	1.23	11.37	$k_{m,pro}$	0.72	9.24
$k_{m,fa}$	0.91	4.34	$k_{m,c4}$	2.12	12.96	$k_{m,pro}$	0.51	8.59	$k_{m,pro}$	0.75	10.21	$k_{m,ac}$	3.56	12.26	$k_{m,ac}$	5.11	17.49	$k_{m,ac}$	4.13	17.22
$k_{m,c5}$	0.22	3.64	$k_{m,pro}$	0.44	10.49	$k_{m,ac}$	7.18	17.17	$k_{m,ac}$	4.67	11.62	$k_{m,h2}$	3.72	13.46	$k_{m,h2}$	4.13	15.65	$k_{m,h2}$	1.46	12.35
$k_{m,c4}$	4.39	17.87	$k_{m,ac}$	3.16	10.71	$k_{m,h2}$	4.07	10.68	$k_{m,h2}$	3.57	11.84	k_d	5.16	15.78	k_d	3.37	9.47	k_d	4.43	13.37
$k_{m,pro}$	0.62	8.62	$k_{m,h2}$	2.60	8.32	k_d	3.67	9.00	k_d	3.22	8.23	$K_{S,Xh2}$	0.13	1.09	$pH_{LL,ac}$	10.24	24.61	$pH_{LL,ac}$	11.69	29.21
$k_{m,ac}$	4.88	16.35	k_d	2.86	7.83	$K_{S,Xh2}$	0.40	1.76	$K_{S,Xh2}$	0.22	0.91	$pH_{LL,ac}$	11.04	25.72	$f_{bu,su}$	3.34	26.74	$f_{bu,su}$	1.89	24.59
$k_{m,h2}$	1.60	11.78	$K_{S,Xh2}$	0.71	2.03	$pH_{LL,ac}$	11.09	22.10	$pH_{LL,ac}$	9.69	18.95	$K_{i,Snh3,Xh2}$	0.21	3.16	$f_{ac,su}$	0.96	13.49	$f_{ac,su}$	0.22	9.58
k_d	1.65	5.26	$pH_{LL,ac}$	11.48	25.57	$K_{i,Snh3,Xh2}$	0.32	2.61	$K_{i,Snh3,Xh2}$	0.39	1.91	$f_{bu,su}$	4.03	30.77	$f_{h2,su}$	5.00	14.87	$f_{h2,su}$	6.37	19.92
$K_{S,Xsu}$	0.05	0.34	$K_{i,Snh3,Xpro}$	0.20	1.79	$f_{bu,su}$	2.72	20.48	$f_{bu,su}$	2.93	24.05	$f_{ac,su}$	0.81	15.33	$X_{ac,Batch7}$	1.89	11.52	$X_{ac,Batch7}$	2.73	13.98
$K_{S,Xaa}$	0.15	1.12	$K_{i,Snh3,Xac}$	0.16	1.55	$f_{ac,su}$	0.41	10.59	$f_{ac,su}$	0.48	12.46	$f_{h2,su}$	7.05	17.03	$X_{h2,Batch7}$	0.00	0.00	-	-	-
$K_{S,Xfa}$	0.15	3.83	$K_{i,Snh3,Xh2}$	0.24	1.70	$f_{h2,su}$	6.02	13.39	$f_{h2,su}$	5.83	13.35	$K_{i,Sh2,Xc4}$	0.03	0.40	-	-	-	-	-	-
$K_{S,Xc5}$	0.07	0.63	$f_{bu,su}$	3.56	30.53	$K_{i,Sh2,Xc4}$	0.33	4.00	$K_{i,Sh2,Xc4}$	0.16	4.36	$X_{ac,Batch7}$	1.63	7.72	-	-	-	-	-	-
$K_{S,Xc4}$	0.00	0.00	$f_{ac,su}$	0.67	17.63	$K_{i,Sh2,Xpro}$	0.17	1.55	$K_{i,Sh2,Xpro}$	0.13	2.88	$X_{h2,Batch2}$	0.07	1.00	-	-	-	-	-	-
$K_{S,Xpro}$	0.00	0.00	$f_{h2,su}$	7.20	16.29	$X_{su,Batch6}$	0.06	0.69	$X_{c4,Batch2}$	0.06	0.28	$X_{h2,Batch6}$	0.00	0.00	-	-	-	-	-	-
$K_{S,Xac}$	0.13	1.13	$K_{i,Sh2,Xfa}$	0.00	0.00	$X_{aa,Batch6}$	0.02	0.38	$X_{c4,Batch6}$	0.06	0.33	$X_{h2,Batch7}$	0.40	3.15	-	-	-	-	-	-
$K_{S,Xh2}$	0.79	4.53	$K_{i,Sh2,Xc5}$	0.03	0.88	$X_{aa,Batch7}$	0.00	0.00	$X_{c4,Batch7}$	0.00	0.00	-	-	-	-	-	-	-	-	-
$pH_{LL,ac}$	6.73	16.94	$K_{i,Sh2,Xc4}$	0.22	2.74	$X_{fa,Batch1}$	0.03	0.10	$X_{pro,Batch1}$	0.05	0.44	-	-	-	-	-	-	-	-	-
$K_{i,Snh3,Xc5}$	0.02	0.29	$K_{i,Sh2,Xpro}$	0.25	2.26	$X_{fa,Batch2}$	0.00	0.00	$X_{pro,Batch2}$	0.00	0.00	-	-	-	-	-	-	-	-	-
$K_{i,Snh3,Xc4}$	0.16	2.64	k_La	0.07	0.39	$X_{fa,Batch6}$	0.00	0.00	$X_{pro,Batch6}$	0.05	0.64	-	-	-	-	-	-	-	-	-
$K_{i,Snh3,Xpro}$	0.33	4.71	$X_{su,Batch1}$	0.05	0.47	$X_{fa,Batch7}$	0.07	0.69	$X_{pro,Batch7}$	0.20	1.12	-	-	-	-	-	-	-	-	-
$K_{i,Snh3,Xac}$	0.99	6.99	$X_{su,Batch2}$	0.03	0.28	$X_{c5,Batch1}$	0.00	0.01	$X_{ac,Batch1}$	0.15	1.09	-	-	-	-	-	-	-	-	-
$K_{i,Snh3,Xh2}$	0.23	3.55	$X_{su,Batch6}$	0.22	3.38	$X_{c5,Batch2}$	0.16	0.72	$X_{ac,Batch2}$	0.14	0.38	-	-	-	-	-	-	-	-	-
$f_{bu,su}$	1.97	24.39	$X_{su,Batch7}$	0.04	0.29	$X_{c5,Batch6}$	0.03	0.14	$X_{ac,Batch6}$	0.16	1.89	-	-	-	-	-	-	-	-	-
$f_{ac,su}$	0.56	13.69	$X_{aa,Batch1}$	0.05	0.60	$X_{c5,Batch7}$	0.07	0.26	$X_{ac,Batch7}$	1.99	7.48	-	-	-	-	-	-	-	-	-
$f_{h2,su}$	4.53	12.54	$X_{aa,Batch2}$	0.00	0.00	$X_{c4,Batch1}$	0.06	0.76	$X_{h2,Batch1}$	0.18	0.74	-	-	-	-	-	-	-	-	-
Σ IE (%) =	40.67	-	-	45.46	-	-	50.46	-	-	46.38	-	-	46.94	-	-	45.57	-	-	44.21	-
Total (%) =	72.37	-	-	75.17	-	-	78.67	-	-	74.74	-	-	72.81	-	-	70.49	-	-	68.79	-

Table 6. Calibration of potentially-identifiable input parameters (θ'): Prior and posterior distributions

Parameter	Units	Initial Value	Initial Evaluation Range		Posterior Parameter Distribution						
			Minimum	Maximum	Mean	Median	Mode	5% Percentile	95% Percentile	Skewness	Kurtosis
$K_{h,pr}$	d^{-1}	0.050	0.005	0.095	0.048	0.048	0.044	0.040	0.057	0.217	2.83
$K_{h,ch,slow}$	d^{-1}	0.0120	0.0012	0.0228	0.0109	0.0108	0.0102	0.0084	0.0137	0.171	2.74
$k_{m,fa}$	d^{-1}	10.0	1.0	19.0	7.3	6.8	6.6	4.6	12.0	1.663	6.93
$k_{m,c5}$	d^{-1}	8.0	0.8	15.2	10.4	10.3	8.6	7.2	13.4	0.084	2.75
$k_{m,c4}$	d^{-1}	13.0	1.3	24.7	19.6	19.5	20.2	15.8	23.6	0.001	2.52
$k_{m,pro}$	d^{-1}	10.0	1.0	19.0	12.2	12.2	13.0	7.1	16.7	-0.148	2.66
$k_{m,ac}$	d^{-1}	16.0	1.6	30.4	24.2	24.5	23.2	18.7	29.4	-0.242	2.32
$k_{m,h2}$	d^{-1}	20.0	2.0	38.0	26.0	25.5	25.1	17.0	36.1	0.077	2.19
k_d	d^{-1}	0.040	0.004	0.076	0.040	0.040	0.045	0.020	0.059	-0.155	2.83
pH_{LLac}		5.8	5.0	6.9	5.4	5.4	5.2	5.0	5.9	0.589	2.73
$X_{ac,Batch7}$	kg COD m^{-3}	-2.523	-3.784	-1.261	-2.648	-2.713	-2.853	-3.574	-1.543	0.303	2.39
$f_{bu,su}$	kg COD kg COD^{-1}	0.50	0.05	0.95	0.54	0.54	0.49	0.38	0.72	0.161	2.67
$f_{ac,su}$	kg COD kg COD^{-1}	0.29	0.03	0.55	0.28	0.29	0.23	0.12	0.43	-0.180	2.73
$f_{h2,su}$	kg COD kg COD^{-1}	0.10	0.01	0.19	0.09	0.09	0.09	0.02	0.17	0.060	2.31

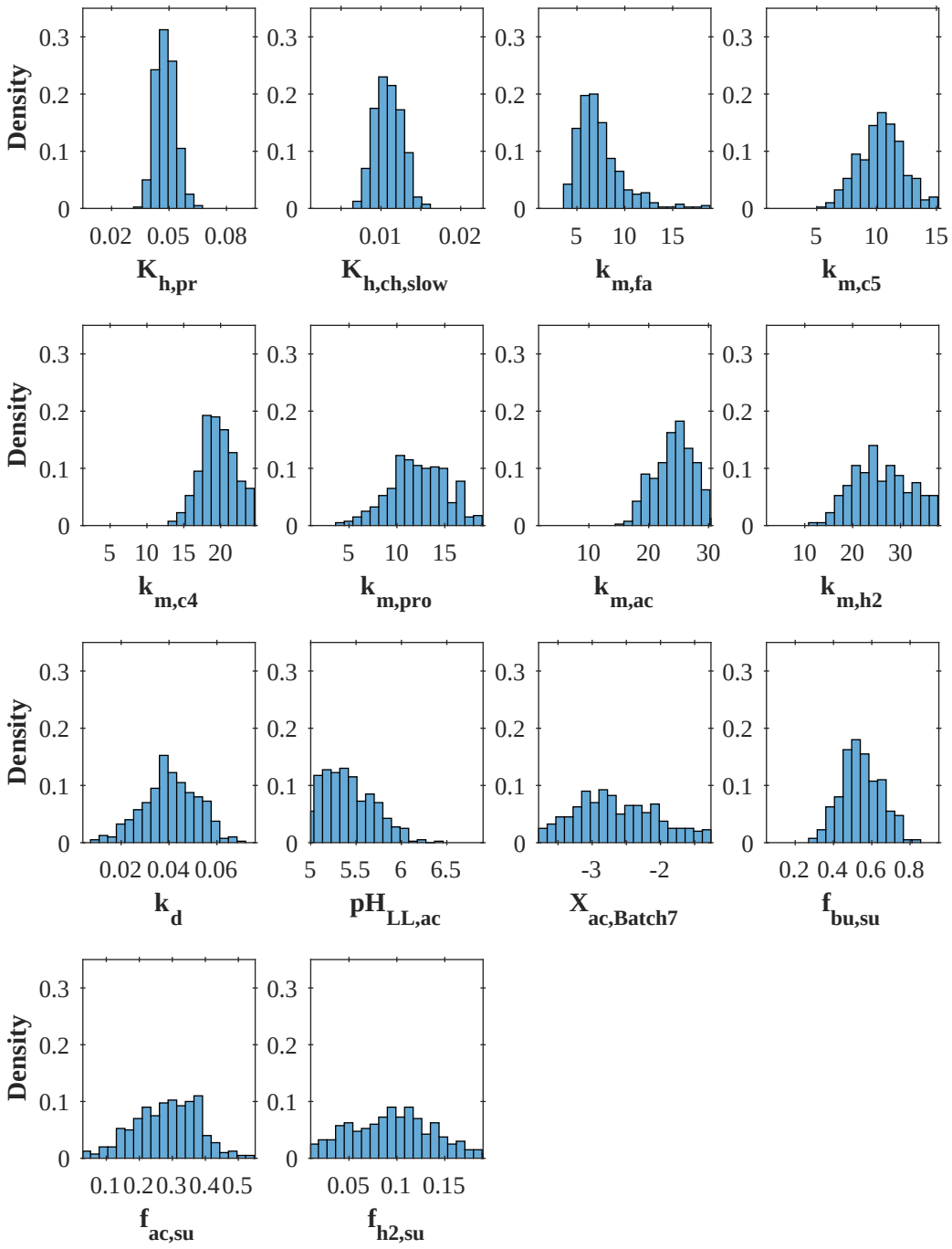

Figure 1. Posterior parameter distributions using 400 simulations and $\varepsilon = 1.05$

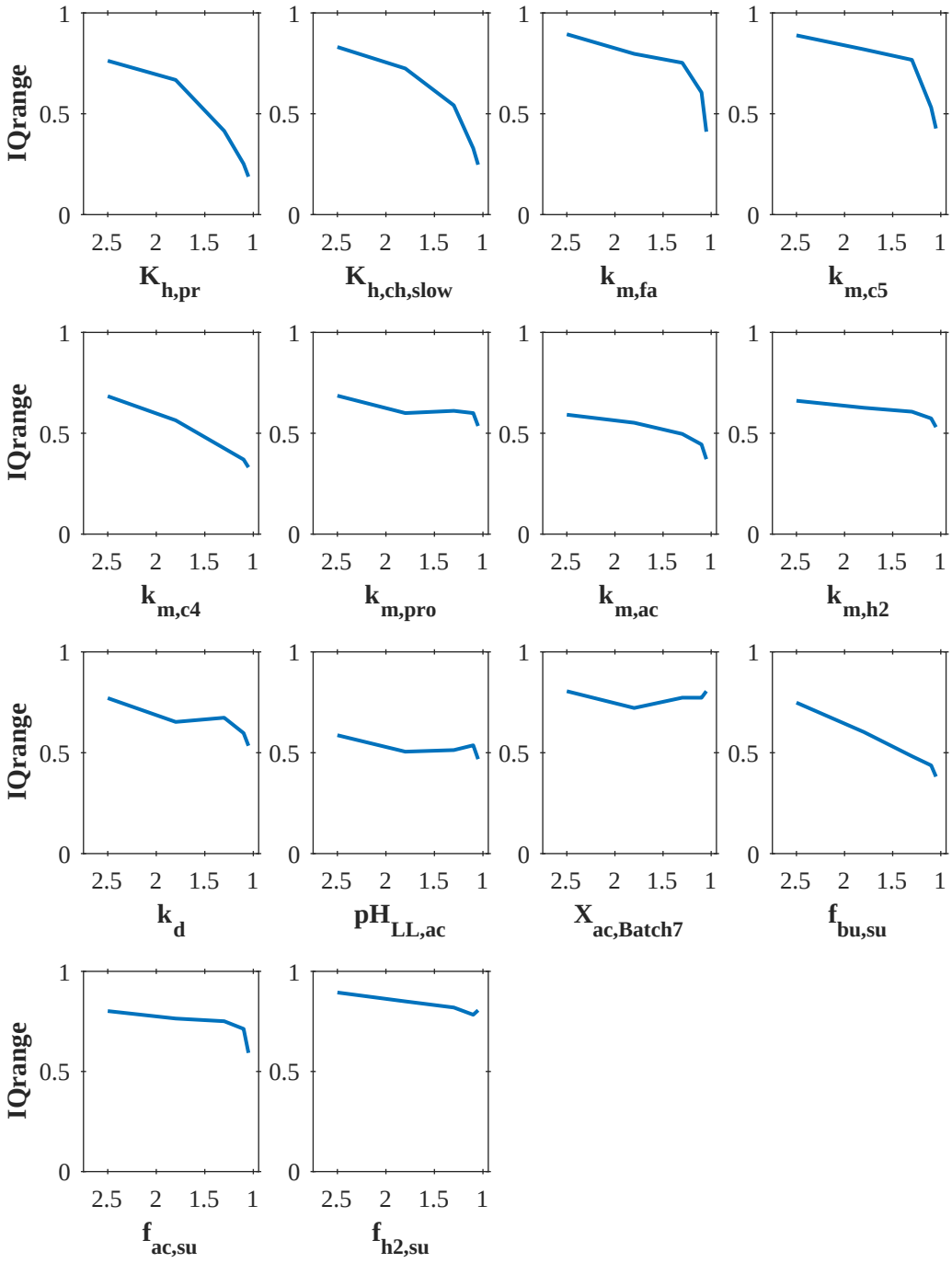

Figure 2. Interquartile range (percentiles 5 to 95 %) of the posterior parameter distributions using $\varepsilon \geq 1.05$ and $\varepsilon \leq 2.50$

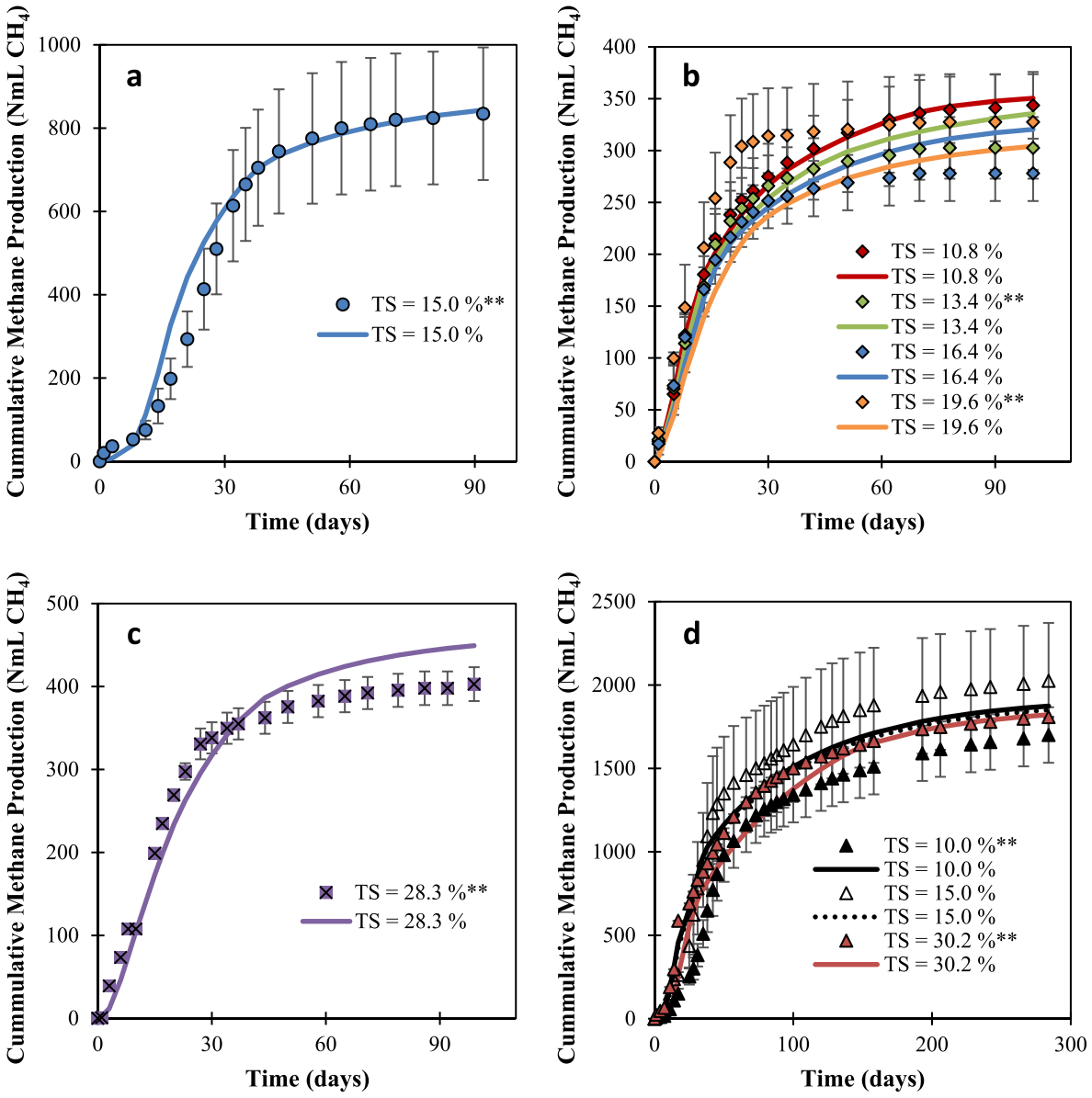

Figure 3. Methane production with mono-digestion of dried OFMSW at a) ISR = 1.00; b) ISR = 1.50; and c) ISR = 1.00; and co-digestion of dried OFMSW and sawdust at d) ISR = 0.16. Dots represent experimental data, while lines represent simulated values.
**Experimental data used for calibration

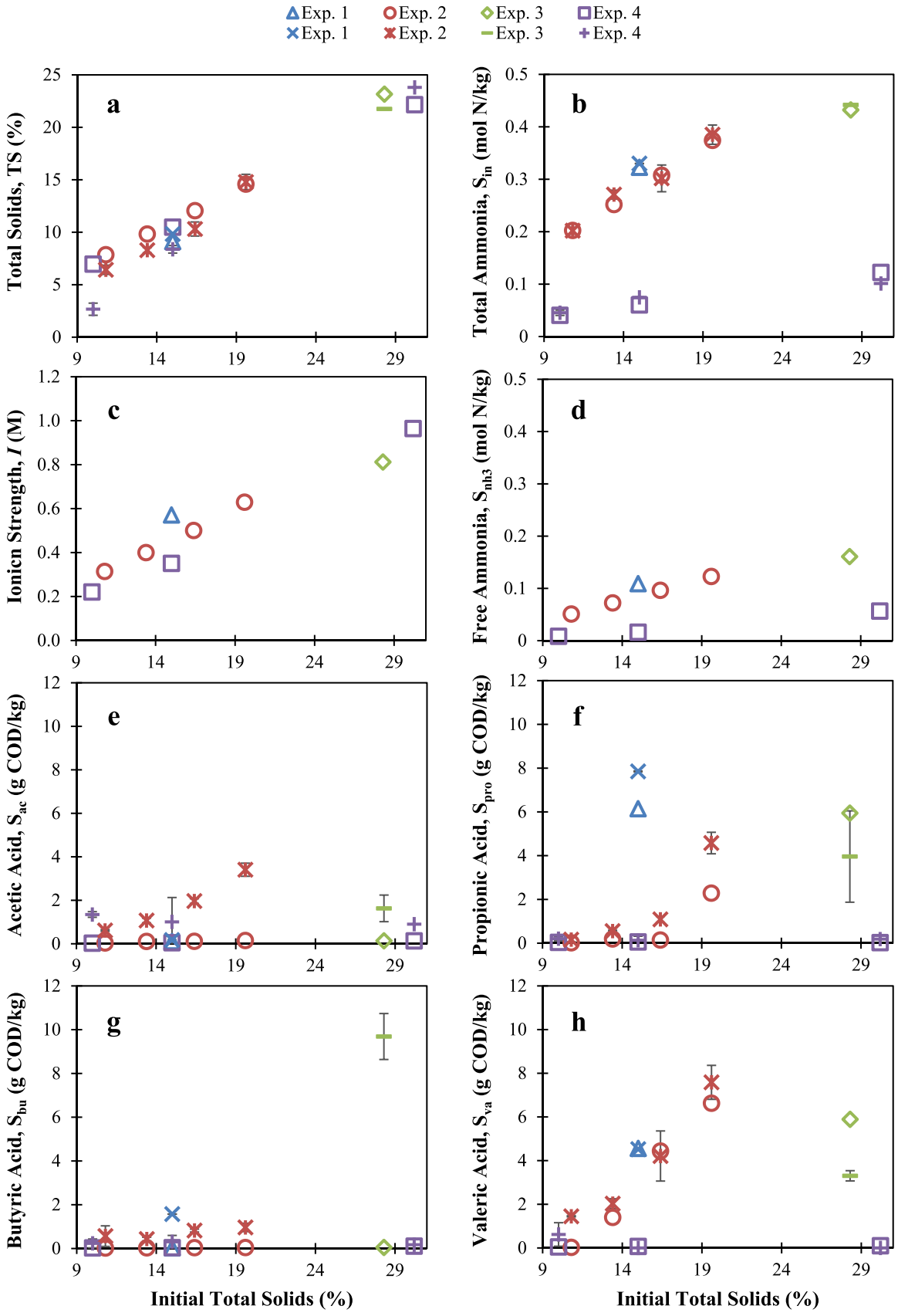

Figure 4. Main variables at the end of the four batch experiments: a) Total solids (TS); b) total ammonia nitrogen (TAN, S_{in}); c) ionic strength (*I*); d) free ammonia nitrogen (NH_3, S_{nh3}); e) acetic acid (S_{ac}); f) propionic acid (S_{pro}); g) butyric acid (S_{bu}); and h) valeric acid (S_{va}). Crosses represent experimental data, while geometries represent simulated values